CZECH TECHNICAL UNIVERSITY IN PRAGUE

FACULTY OF BIOMEDICAL ENGINEERING
Department of Biomedical Technology

Numerical model of microwave heating of different types of tumours

Numerický model mikrovlnného ohřevu různých typů nádorů

MASTER'S THESIS

Study Program:	Biomedical and Clinical Technology
Field of Study:	Biomedical Engineering

Author:	Bc. Anna Pézlová
Supervisor:	Dr.-Ing. Jan Vrba, MSc.

Kladno 2016

Depatment of Biomedical Technology

Academic year: 2015/2016

Diploma Thesis assignment

Student: **Bc. Anna Pézlová**
Study branch: Biomedical engineer
Title: **Numerical model of microwave heating of different types of tumours**
Title in Czech: Numerický model mikrovlnného ohřevu různých typů nádorů

Instructions for processing:

Create numerical models describing local microwave heating of different tumour types based on their blood supply. Examine two following tumour types: a tumour, which lies directly on a blood vessel, and a tumour being supplied from its surface. Based on the numerical models simulating electromagnetic field distribution, heat transfer and blood flow, execute the following parametric analysis. For both above-mentioned tumour types consider three different tumour diameters and three different positions from the skin/water bolus interface. Use COMSOL Multiphysics model environment for creating the numerical models and performing the simulations. Assemble an experiment for verifying the first mentioned numerical model and compare the simulation results with the experiment 's outcome. In the experimental setup use a heterogeneous agar model as a phantom of the treated area and replace blood by saline. For the purpose of numerical simulation results and measured data comparison adjust the numerical simulation to the experimental setup possibilities (in terms of bloodstream and dielectric parameters).

References:

[1] C. A. Balanis, Advanced Engineering Electromagnetics, ed. Solution Manual, Wiley, 1989, Chapter 2, ISBN 0471621943.
[2] J. Vrba, Lékařské aplikace mikrovlnné techniky, ed. 1st, ČVUT Praha, 2003, ISBN 80-01-02705-8.
[3] Rodrigues, Dario B., Hurwitz, Mark D., Maccarini, Paolo F., Stauffer, Paul R., Optimization of chest wall hyperthermia treatment using a virtual human chest model, Antennas and Propagation (EuCAP), 2015 9th European Conference on, ročník 1, číslo 1, 2015, Duben, 1-5 s.
[4] R. K. Jain and K. Wardhartley, Tumor blood-flow - characterization, modifications, and role in hyperthermia, IEEE Transactions on Sonics and Ultrasonics, ročník 31, číslo 5, 1984, 504-526 s.

Validity of Thesis Assignment: 20. 8. 2017
Supervisor: Dr.-Ing. Jan Vrba, MSc.

.....
Head of Department

.....
Dean

In Kladno 23. 02. 2016

Katedra biomedicínské techniky

Akademický rok: 2015/2016

Zadání diplomové práce

Student:	**Bc. Anna Pézlová**
Studijní obor:	Biomedicínský inženýr
Téma:	**Numerický model mikrovlnného ohřevu různých typů karcinomů**
Téma anglicky:	Numerical model of microwave heating of different types of tumors

Zásady pro vypracování:

Vytvořte numerické modely lokálního mikrovlnného ohřevu různých typů karcinomů z hlediska jejich zásobování krví. Uvažujte dva následující typy karcinomů, karcinom, kterým céva prochází, a karcinom, který je zásobován krví ze svého povrchu. Pomocí Vámi vytvořených vázaných numerických modelů umožňujících současně simulovat rozložení elektromagnetického pole, transfer tepla a proudění krve cévou proveďte následující parametrickou analýzu. Pro oba výše uvedené typy karcinomu uvažujte tři různé průměry nádorů a tři různé polohy nádorů od rozhraní kůže/vodní bolus. K vytvoření numerických modelů a provedení simulací použijte prostředí COMSOL Multiphysics. Sestavte experiment pro ověření prvního výše zmíněného numerického modelu a porovnejte data získaná simulacemi s výsledky experimentu. V experimentálním uspořádání použijte jako fantom léčené oblasti homogenní agarový fantom a místo krve solný roztok. Pro účely porovnání výsledků numerických simulací a naměřených dat přizpůsobte numerický model možnostem experimentu (z hlediska krevního řečiště a dielektrických vlastností).

Seznam odborné literatury:

[1] C. A. Balanis, Advanced Engineering Electromagnetics, ed. Solution Manual, Wiley, 1989, Chapter 2, ISBN 0471621943
[2] J. Vrba, Lékařské aplikace mikrovlnné techniky, ed. 1st, ČVUT Praha, 2003, ISBN 80-01-02705-8
[3] Rodrigues, Dario B., Hurwitz, Mark D., Maccarini, Paolo F., Stauffer, Paul R., Optimization of chest wall hyperthermia treatment using a virtual human chest model, Antennas and Propagation (EuCAP), 2015 9th European Conference on, ročník 1, číslo 1, 2015, Duben, 1-5 s.
[4] R. K. Jain and K. Wardhartley, Tumor blood-flow - characterization, modifications, and role in hyperthermia, IEEE Transactions on Sonics and Ultrasonics, ročník 31, číslo 5, 1984, 504-526 s.

Vedoucí:	Dr.-Ing. Jan Vrba, MSc.
Konzultant:	Ing. David Vrba, Ph.D.

Zadání platné do: 20.08.2017

.....
vedoucí katedry / pracoviště

.....
děkan

V Kladně dne 22.02.2016

Declaration

I hereby declare that I have developed and written the enclosed Master's Thesis titled:
Numerical model of microwave heating of different types of tumours
completely by myself, and have not used sources or means without declaration in the text. Any thoughts from others or literal quotations are clearly marked and list of references is enclosed.
I have no objection to the usage of this work in compliance with the act §60 of Law No.121/2000 Coll. about copyright and laws related to the copyright and about the changes of certain laws.

In Kladno ....

Anna Pézlová

Prohlášení

Prohlašuji, že jsem diplomovou práci s názvem:
Numerický model mikrovlnného ohřevu různých typů nádorů
vypracovala samostatně a použila k tomu úplný výčet citací použitých pramenů, které uvádím v seznamu přiloženém k práci.
Nemám závažný důvod proti užití tohoto školního díla ve smyslu §60 Zákona č.121/2000 Sb., o právu autorském, o právech souvisejících s právem autorským a o změně některých zákonů (autorský zákon).

V Kladně dne ....

Anna Pézlová

Acknowledgements

I would like to express my gratitude to my supervisor Dr.-Ing. Jan Vrba, MSc. for the useful comments, remarks and engagement through the learning process of this Master's Thesis. Furthermore I would like to thank Ing. David Vrba, Ph.D. for advising me in the absence of my supervisor.

Master's Thesis title

Numerical model of microwave heating of different types of tumours.

Abstract

The knowledge of complete temperature distribution throughout heated tissues is crucial in designing efficient hyperthermia treatment for cancer. The cooling effect of large blood vessels may cause inhomogeneity in temperature distribution and possible underdose, which may later lead to tumour re-growth. The aim of this thesis is to create multiple numerical simulations describing local microwave heating of two different tumour types based on their blood supply – a tumour, which lies directly on the blood vessel and a tumour being supplied from its surface. The next aim is to validate correct parameter settings in the simulations experimentally. In this thesis, numerical models of a tumour lying on a blood vessel and a tumour being supplied from its surface have been developed to calculate the temperature distribution in tissue during microwave hyperthermia treatment. Furthermore, a heterogeneous agar model was created and used in an experiment validating the settings of the numerical simulations. The used thermal model is based on bioheat transfer equation describing heat transfer in perfused tumour and surrounding tissue. Equations were solved in COMSOL Multiphysics by finite element method. As results of the simulations, tumours supplied from their surface are being heated more easily and complete tumour necrosis can be achieved with hyperthermal treatment. Compared to that, tumours lying directly on a blood vessel need more output power to be heated to desired temperatures, which brings higher possibility of surrounding tissue damage.

Keywords

Microwave hyperthermia; numerical simulaton; tumour vasculature

Název diplomové práce

Numerický model mikrovlnného ohřevu různých typů nádorů

Abstrakt

Při navrhování efektivní onkologické léčby metodou mikrovlnné hypertermie je nezbytná znalost kompletního teplotního rozložení v léčené oblasti. Schopnost velkých cév ochladit okolní tkáň může ovlivnit teplotní rozložení a způsobit nedostatečné prohřátí, což může později vést ke zpětnému dorůstání nádoru. Cílem této práce je vytvořit numerické simulace popisující mikrovlnný ohřev dvou různých typů nádorů v závislosti na jejich cévním zásobení - nádor, kterým céva prochází, a nádor, který je zásobován krví ze svého povrchu. Dále je cílem experimentálně ověřit správné nastavení simulací. V této práci byly vytvořeny numerické modely nádoru, kterým céva přímo prochází, a nádoru zásobeného ze svého povrchu, které slouží k výpočtu teplotního rozložení při léčbě metodou mikrovlnné hypertermie. Dále byl vytvořen heterogenní agarový model tkáně, který byl použit pro experimentální ověření nastavení numerických simulací. Použitý model je založen na rovnici přestupu tepla popisující přenos tepla mezi nádorem a okolní zdravou tkání. Rovnice byly řešeny v programu COMSOL Multiphysics metodou konečných prvků. Z výsledků vyplývá, že se nádory zásobené ze svého povrchu ohřívají snadněji a metodou mikrovlnné hypertermie je možné u nich dosáhnout kompletního zničení. Nádory, kterými céva prochází, mají oproti tomu vyšší nárok na výkon nutný k jejich ohřátí na požadovanou teplotu, což s sebou nese možnost většího poškození okolní tkáně.

Klíčová slova

Mikrovlnná hypertermie; numerická simulace; cévní zásobení nádoru

Contents

List of Acronyms

Acronym	Meaning
CT	Computed Tomography
DIVA	Discrete Vasculature
i.d.	inner diameter
MR	Magnetic Resonance
PE	Polyethylen
RPM	Rounds per Minute
SAR	Specific Absorption Rate
VEGFs	Vascular Endothelial Growth Factors
VTAs	Vascular Targeting Agents

List of Symbols

Symbol	Unit	Meaning
σ	S/m	Electric conductivity
ρ	$(\mathrm{kg/m^3})$	Density
k	$(\mathrm{W/(m \cdot K)})$	Thermal conductivity
ϵ	–	Relative permittivity
ω_b	1/s	Blood perfusion rate
C_p	$(\mathrm{J/(kg \cdot K)})$	Specific heat
ρ_b	$(\mathrm{kg/m^3})$	Blood density
C_b	$(\mathrm{J/(kg \cdot K)})$	Specific Heat Capacity of Blood
T_b	K	Arterial Blood Temperature
Q_{met}	$(\mathrm{W/m^3})$	Metabolic Heat Source
Q_{ext}	$(\mathrm{W/m^3})$	External Heat Source

1 Introduction

Tumour diseases figure among the leading causes of death worldwide. Development of new therapies and improvements of existing cancer treatment methods are therefore highly demanded.

Microwave hyperthermia is a cancer treatment method like surgery, chemotherapy and radiotherapy. It uses microwaves to heat the tissue in order to destroy the cancer cells. Its greatest advantages are the use of non-ionizing radiation and the non-invasiveness of the method. It can be used independently, but best results are delivered in combination with chemotherapy and radiation therapy.

The use of heat in medicine and cancer treatment is not a completely new concept. Already in 1866 a German physician Dr. W. Busch reported the disappearance of a facial sarcoma in a patient suffering from high fevers [1]. Modern hyperthermia uses elevated temperatures for destroying tumour cells due to the unorganized vascular system of these, which makes them less resistant to heat. The temperature rise can be achieved by lasers, ultrasound or microwaves. Along with the temperature the blood circulation and tissue perfusion increases. This phenomenon is utilized in combination with chemotherapy, in which the increased perfusion of the tumour can ensure better regional efficacy of the medication used.

For the clinical use of microwave hyperthermia the treatment planning is crucial. This is necessary for design, control and evaluation of the treatment. One of the most difficult problems during treatment planning is the determination of the complete temperature field in the tumour and also in surrounding healthy tissues. Such determination is very important for evaluating the treatment efficacy. To be able to compute the complete temperature distribution, it is possible to use mathematical models and computer simulations. In these numerical simulations it is essential to also consider the possible effect of larger vessels on the treatment. Large blood vessels can produce localized cooling in heated tissues during hyperthermia treatment, causing inhomogeneities in the temperature distribution in the tissue, and thereby a decrease of the treatment efficacy [2].

The computed heat distribution during the hyperthermia treatment should be then tested on a suitable real object before being applied directly to patients. Agar phantoms are very often being used for these purposes, because their material properties and behaviour during thermotherapy are very similar to those of real human tissue.

1.1 Microwave thermotherapy

Microwaves are widely used in medicine, both in diagnostic and therapeutic applications. Treatment methods based on the thermal effect of microwaves are referred to as microwave thermotherapy. This can be further divided according to the goal temperature or interval achieved during therapy. Diathermia is heating of tissue to the temperature of 41°C and is used for chronic pain and inflammation treatment. Hyperthermia stands for heating to the goal interval of 41°C – 45°C, using the principle of a different biological response of healthy and tumour tissue and so can be used for cancer treatment. In cancer therapy is hyperthermia often used as an adjunct to chemotherapy and radiation therapy. An application in urology, used for prostate treatment, is microwave thermocoagulation (thermoablation), which uses temperatures higher than 45°C. Among other applications can be also mentioned microwave scalpel used in surgery and microwave tomography used for tumour detection based on differences in tissue electrical properties as a representation from the field of diagnostics.

1.2 Biological effects of microwave energy

Microwaves are a form of electromagnetic radiation with frequencies from 300 MHz to 300 GHz. This corresponds to wavelength in the range between 1 mm and 10 cm. Their long-term effect on the human organism is still being discussed as the problem is very complex and the effects are dependent on many factors and circumstances. However, no long-term effects of microwaves on the organism have been proven yet. Biological effects of microwave energy can be divided into two main groups: thermal and non-thermal effects [3].

Thermal effects

Thermal effects of microwaves are caused by absorption of microwave radiation in the irradiated tissue. The absorption is dependent on many factors such as frequency, orientation and polarization of the radiation, electrical and magnetic field intensity and dielectric parameters of interacting tissues. Those effects are accompanied by physiological responses, which are dependent on the intensity and duration of the field [3].

Non-thermal effects

There is no heating of the tissue at a low energy level of the electromagnetic field. No noxiousness of the non-thermal effects of microwave energy has been proven in studies conducted in vitro on living cells, but it is still a subject of discussion [3].

The rate of power absorbed in the biological tissue is often expressed using Specific absorption rate (SAR). This dosimetric parameter is an indicator of energy amount dissipated in the tissue. It is defined as power absorbed per 1 kg of tissue. SAR indicates the electromagnetic field exposure rate of biological tissue very precisely, but is difficult to measure. Therefore it is often computed using the Eq. 1,

$$SAR = \frac{\partial}{\partial t}\left(\frac{\partial W}{\partial m}\right) = \frac{\partial}{\partial t}\left(\frac{\partial W}{\rho \partial V}\right) = \frac{\partial P}{\partial m} = \frac{\partial P}{\rho \partial V} \tag{1}$$

where W is electromagnetic energy absorbed in biological tissue, t is time, m represents mass. P stands for the power of electromagnetic wave passing through the biological tissue, ρ is tissue density and V is the tissue volume.

1.3 Principles of hyperthermia

Hyperthermia is based on the principle of different biological response to heating of healthy and tumour tissue. Healthy tissue has a reflexive defence mechanism of increasing blood circulation in order to cool down the heated tissue. This mechanism protects the healthy tissue from thermal damage up to 45°C. Several experiments have shown that the tissue perfusion is temperature dependent. In healthy tissue, when heated up to 45°C, the blood flow continuously increases in order to protect the tissue from further heating. On the contrary, tumour tissue shows a decrease in blood flow when heated and due to irregular and chaotic vasculature, which hinders the perfusion and enhances further temperature increase. Tumour tissue is therefore being damaged already at 41°C. Diameter of blood vessels can increase in healthy tissue due to the local response which dilates the heated vessels by relaxing vascular smooth muscles. But neoplastic tumour vasculature lacks this mechanism due to the lack of smooth muscles [4]. The different temperature curves for healthy and tumour tissue can be seen in Fig. 1. In all tissues, for temperatures above 45°C, blood flow decreases due to irreversible damages in the vasculature [5].

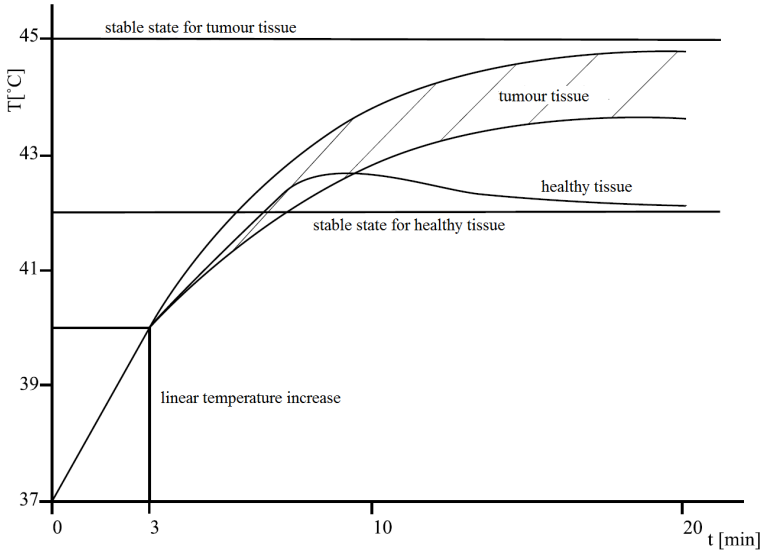

Figure 1: Temperature curves for tumour and healthy tissue with identical heating conditions. Taken from [3], translated.

1.4 Hyperthermia treatment planning

Despite the promising potential of hyperthermia treatment proven in numerous studies, it has so far failed to gain widespread acceptance. This might be due to the difficulty of providing reliable heating of the entire tumour while reducing energy absorption in healthy tissue, caused by complexity of the applicators and no straightforward relationship between the treatment settings and the resulting temperature distribution. The goal of hyperthermia treatment planning is therefore to solve this problem and help to visualize the course of the treatment [6].

In order to maximize the treatment effectiveness, reliable information about spatial power distribution and temperature during hyperthermia treatment is essential. One of the biggest challenges during clinical hyperthermia is the determination of the complete 3D temperature field throughout the treatment area, including both healthy and tumour tissue. Thus the complex relation between heating, tissue perfusion, vasculature and anatomical structures needs to be considered. Also blood perfusion plays an important role in temperature distribution. Therefore it is important to take vasculature into consideration during hyperthermia treatment planning. Temperature and power distribution is usually non-uniform, due to heterogeneous thermal and dielectric tissue properties. As heat removal by blood flow is also non-uniform, it only contributes to the heterogeneity

of temperature distribution [7].

Typical frequencies used in microwave hyperthermia treatment are 434 MHz, 915 MHz and 2450 MHz. The last is used for superficial treatments as it only allows heating to a depth of 1.5 cm in muscle tissue. Frequency 434 MHz is used for local subsurface treatments in depths between 2 and 4 cm in muscle tissue [3].

There are several models of various complexity used for the purpose of treatment planning. The most used model is Penne's bioheat equation:

$$\rho C_p \frac{\partial T}{\partial t} + \nabla \cdot (-k \nabla T) = C_b \omega_b \rho_b (T_b - T) + Q_{met} + Q_{ext}, \tag{2}$$

where C_p is the specific heat capacity of the tissue (J/(kg·K)), k is the tissue thermal conductivity (W/(m·K)), ρ_b represents the blood density (kg/m^3), C_b is the specific heat capacity of blood (J/(kg·K)), ω_b blood perfusion rate (1/s), T_b represents arterial blood temperature (K), Q_{met} is the metabolic heat source (W/m^3) and Q_{ext} is an external heat source (W/m^3) [8].

This bioheat equation uses a heat sink proportional to the local temperature rise and a non-directional volumetric average perfusion rate. Its weakness is that it does not consider the direction of blood flow. Basic vasculature models are relatively simple with blood vessels represented as straight tubes of a specified inner diameter. These models are used to compute temperature distribution during thermal treatment or ablation [7].

More advanced models are in 3D with branching vessel network and provide a more complex description of the temperature field. In the sophisticated discrete vasculature (DIVA) model the vessel-network is described by 3D curves with a specified diameter, so it allows more precise thermal modelling. This model is compatible with MR/CT angiography vessel reconstruction software, which is important for routine use in hyperthermia treatment planning. The DIVA model was validated experimentally by using isolated perfused animal tissue (tongue) and this comparison showed an excellent agreement [7].

Hyperthermia treatment planning helps to optimize the generated temperature distribution within the patient's body to a level, where essentially the tumour is heated, but preferably not any normal tissue is damaged. For this reason, patient-specific treatment planning is necessary. In order to achieve this, prospective treatment planning is used. Detailed knowledge of the particular patient's anatomy is needed in order to be able to compute the power deposition patterns in the tissue and provide individual patient treatment planning. Prospective hyperthermia treatment planning can noticeably improve the

effectiveness and quality of the treatment [6, 9].

The electromagnetic field distribution in the patient is calculated by numerically solving Maxwell equations. Absorbing boundary conditions are essential for the models in order to avoid reflections of the electromagnetic waves at the boundaries of the computational domain. In order to obtain the required solutions, it is desirable to use numerical simulations. Besides a number of commercially available dedicated treatment planning software packages (i.e. Sigma HyperPlan or Sim4Life), electromagnetic calculations and thermal simulations for hyperthermia treatment planning can be executed using general purpose commercial software packages such as COMSOL Multiphysics, Ansys High Frequency Structural Simulator and CST STUDIO SUITE. These software packages provide flexibility in applicator modelling, but supplementary software is required for tissue segmentation and treatment optimization [9].

1.5 Tumour vasculature

In order to study the temperature distribution in tumour tissue during hyperthermia treatment, it is necessary to outline the fundamental principles of tumour angiogenesis, vasculature morphology and its role in hyperthermia.

It is widely accepted that most tumours and metastases originate as small avascular mass formations that induce the development of new blood vessels once they grow to a few millimetres (around 2 mm) in size. Initial avascular growth is typical for tumours that arise in epithelial structures and are separated from the underlying vasculature by a basement membrane [10] .

Tumour vasculature has abnormal morphology with unstable and devious blood vessels. This phenomenon can be used in treatments, where tumour blood vessels are targeted in order to suppress tumour growth. They can be selectively destroyed without affecting normal blood vessels.

1.6 Angiogenesis

Tumours need blood supply in order to grow. They have to develop their own functional blood supply from the already established healthy tissue vasculature. The process of new blood vessels creation from already existing vessels is called angiogenesis. It is initiated by local hypoxia (decreased availability of oxygen to the body tissues), which activates vas-

cular endothelial growth factors (VEGFs), that can stimulate endothelial-cell growth [11]. In the absence of angiogenesis, tumour growth is restricted. Therefore tumour dimensions are limited to a microscopic size of 1-2 mm. At this magnitude simple diffusion of nutrients and waste products becomes limiting for continuous development of the tumour. Such avascular growth is characteristic for tumours separated from the blood vessels by a membrane, i.e. tumours in early development stage originating in epithelial tissue [12].

Initiation of tumour angiogenesis is signalized by structural destabilization of already existing blood vessels. Endothelial cells migrate under the influence of VEGFs secreted by the tumour towards the tumour cells and it comes to creation of new blood vessels. This process leads to a loss of hierarchic composition of large, middle sized and small blood vessels as found in the normal vascular system, which is the reason why tumour vessels have irregular shape and diameter, they are devious, leaky and often have dead ends. The resulting arrangement of tumour vasculature is therefore insufficient in terms of metabolic demands of the tissue. Later, tumour blood vessels will go through stabilization and remodelling process. During this process, the dense network of immature and chaotically organized blood vessels clumps together and form blood vessels with increased diameter. This happens in the middle of the tumour and leads to a better arrangement of vasculature and blood supply in the tumour, but on the contrary also to a local necrosis of the tissue inside the tumour core [13, 14]. The stabilization process can be seen in Fig. 2.

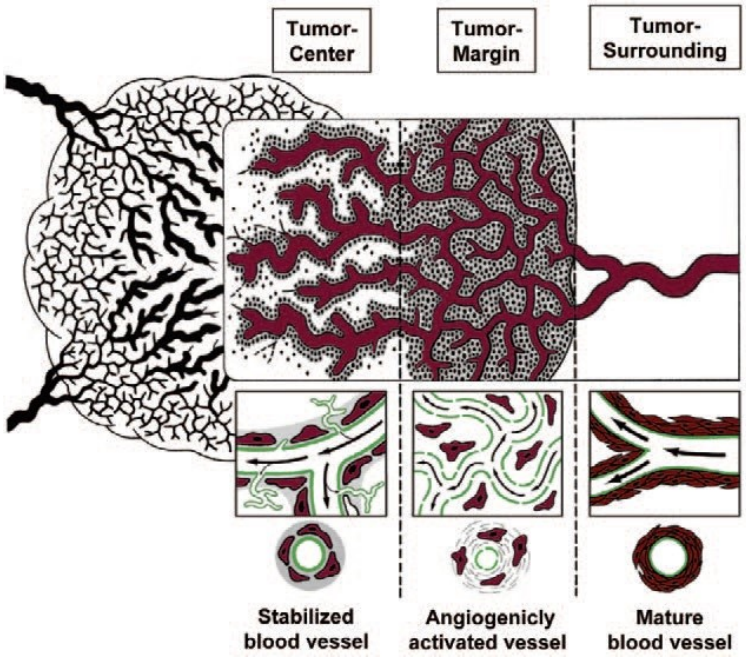

Figure 2: Blood vessel stabilization in the tumour centre associated with extended necrosis of tumour tissue. Taken from [13].

1.7 Tumour blood flow

The tumour neovasculature is not only critical for survival of the tumour cells, but it is also probably one of the most important factors influencing the therapeutic application of hyperthermia. As blood flow is one of the major means by which heat can be dissipated from perfused tissues, the vasculature is a target for hyperthermia damage. Generally, the lower the rate of blood flow, the easier it is to heat. Therefore sometimes the concept of vascular targeting agents (VTAs) is being used as a therapeutic approach in order to disrupt the tumour vasculature and hereby facilitate regional heating.

As the tumour neovasculature has a very different structure from the normal vessels, it is unable to meet all oxygen and nutrient needs of the growing tumour; therefore some areas in the tumour mass can become oxygen deprived, nutrient deficient, and highly acidic. When a neoplastic tissue is heated, lactic acid accumulates and hence, the pH decreases within the tissue. This decrease in pH increases vascular destruction. Cells existing in such conditions are then even more sensitive to the cytotoxic action of heat [15].

The blood supply to tumours is spatially heterogeneous, and it decreases, in general, as the tumour grows larger. Because of blood flow heterogeneities, even the poorly perfused tumours may have regions of high perfusion rate making it difficult to heat these tumours effectively [4].

1.8 Thesis aims and objectives

The aim of this thesis is to create multiple numerical simulations describing local microwave heating of two different tumour types based on their blood supply - tumour, which lies directly on the blood vessel and tumour being supplied from its surface. Simulations of electromagnetic field distribution, heat transfer and blood flow for tumours of three different diameters placed in various depths under the skin will be made in COMSOL Multiphysics. Furthermore, an agar phantom is to be created and used in an experiment. The aim of the agar phantom experiment is to validate correct material parameter and boundary settings in the numerical simulations. Generator output power and water bolus temperature will be regulated in the numerical simulations. The goal of this regulation is adjustment of the simulated temperature distribution in the tissue aiming a treatment outcome optimization.

2 Methods

Three different numerical simulations of a spherical tumour located in various tissues were designed. Two models represent tumour, which lies directly on the blood vessel, and tumour being supplied by blood and nutrients from its surface. The third model is a modified version of tumour lying directly on the blood vessel. This model was used to evaluate results from measurement on a heterogeneous agar phantom, which consisted of more layers of agar representing different human body tissues. The agar model was created for the purpose of experimental validation of settings of the former two computational models. The model was therefore simplified according to the experimental setup possibilities.

2.1 Experimental setup

Experiment was conducted using a heterogeneous agar phantom consisting of mixture of tumour, blood vessel, muscle tissue, subcutaneous fat and skin. Vessel was imitated using a PE tube with inner diameter of 2 mm and wall thickness of 0.5 mm. The rest of tissues were simulated with agarose and different ingredients.

Tumour phantom

Tumour phantom consists of:

- 100 mL of distilled water
- 60 mL of 96% ethanol
- 4 g of agarose
- 2.9 g of NaCl
- 0.1 g of food colouring

Distilled water, ethanol, salt and food colouring were mixed in a pot and heated. At a temperature around 80°C agarose was added to the mixture and everything was stirred for one minute and then poured in a prepared mold letting it to solidify directly on the tube representing blood vessel. The final sample as well as the mold can be seen in Fig. 3.

Directions were taken from the article [16] with a slight modification - the agarose percentage in the mixture was increased after performing some testing samples and in

accordance with work [17]. This alternation was introduced in order to improve the phantom texture so, that it holds together more and can be used for creating a heterogeneous phantom.

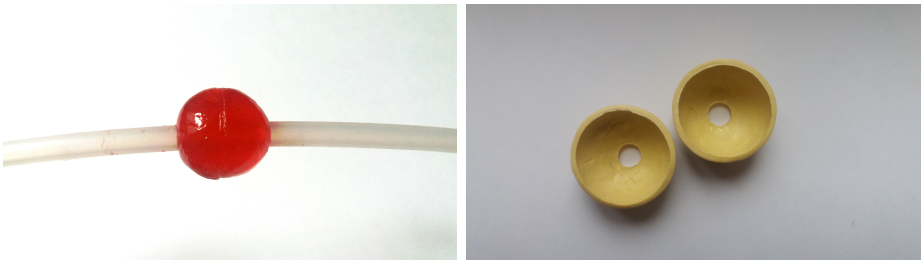

Figure 3: Prepared tumour phantom on a PE tube (left) and the mold used (right).

Muscle phantom

The agarose mixture representing muscle tissue contained:

- 2800 mL of water
- 9.7 g of NaCl
- 117 g of agarose

All ingredients were mixed together and heated until the final mixture started to abruptly change its density. Then the mixture was poured into a mold letting the mixture to solidify. Directions were taken from [17], only tap water was used instead of deionized water. Measured dielectric properties of the phandom made of deionized or tap water did not show any difference.

Fat phantom

Layer representing subcutaneous fat consisted of:

- 134 g of wheat flour
- 60 g of sunflower oil
- 5.94 g distilled water
- 0.06 g of NaCl

All ingredients were mixed in a bowl and the resulting dough was kneaded until it was elastic and smooth on the outside. Then the dough was spread in a thin layer on the already solidified agar muscle phantom. Directions were taken from [17].

Composition of the skin phantom was the same as for the muscle phantom, as skin and muscle tissues have very similar dielectric parameters. Agarose mixture representing skin was then poured at the top of the fat layer. The final heterogeneous agar phantom can be seen on Fig. 4.

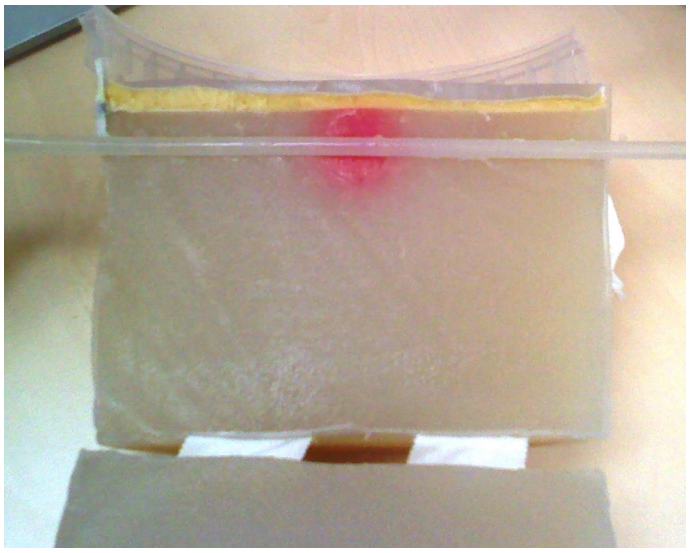

Figure 4: Prepared heterogeneous agar phantom; a cross section.

A sample was taken from each component of the heterogeneous phantom and its dielectric parameters were measured (Fig. 5) to be used later in the numerical simulation. This measurement was performed using DAK-12 coaxial dielectric probe (Schmid & Partner Engineering AG) connected to KEYSIGHT FieldFox N9923A vector network analyzer. Dielectric parameters were measured in the 10 MHz – 3 GHz frequency range. Results of measurements for the complete frequency range can be found in Attachment n. 1 . For the simulations were used dielectric parameters measured on the frequency of 434 MHz.

The experimental setup consisted of the heterogeneous agar model, peristaltic pump FH100 from Thermo Scientific, two reservoir bottles, silicone tubing with connectors attaching the tube inside the phantom to the rest of the tubing and a wave generator with rectangular waveguide applicator with aperture dimensions 7.5×10 cm. Scheme of the experimental setup is presented in Fig. 6. The final thermographic picture was taken by thermographic camera FLIR E60 (FLIR Systems AB, Eskilstuna, Sweden).

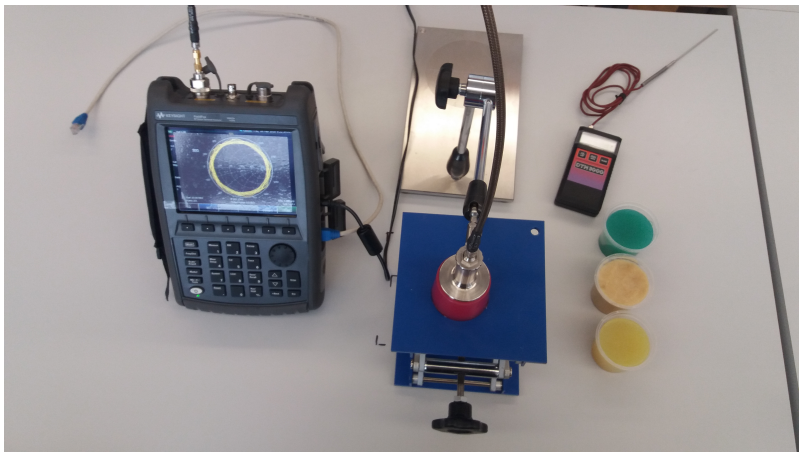

Figure 5: Experimental setup during measurement of dielectric parameters with coaxial dielectric probe and vector network analyzer.

Experiment was performed after temperature stabilization of all model components at 23°C, as it was not possible to keep all components tempered at body temperature. Blood was replaced by saline (9 g of salt per 1 L of water) for experimental purposes and pumped by a peristaltic pump set to 400 RPM through the circuit. This setting provided saline flow of 1 cm/s, which was calculated using the pump datasheet and verified experimentally. The output power of the microwave generator was set to 100 W and exposition time was two minutes. After this time, applicator was removed, agar phantom was placed under a thermographic camera, cut in half along the vessel and opened and thermographic images of the cross section were taken. This procedure needed to be performed as quickly as possible in order to minimize heat loss.

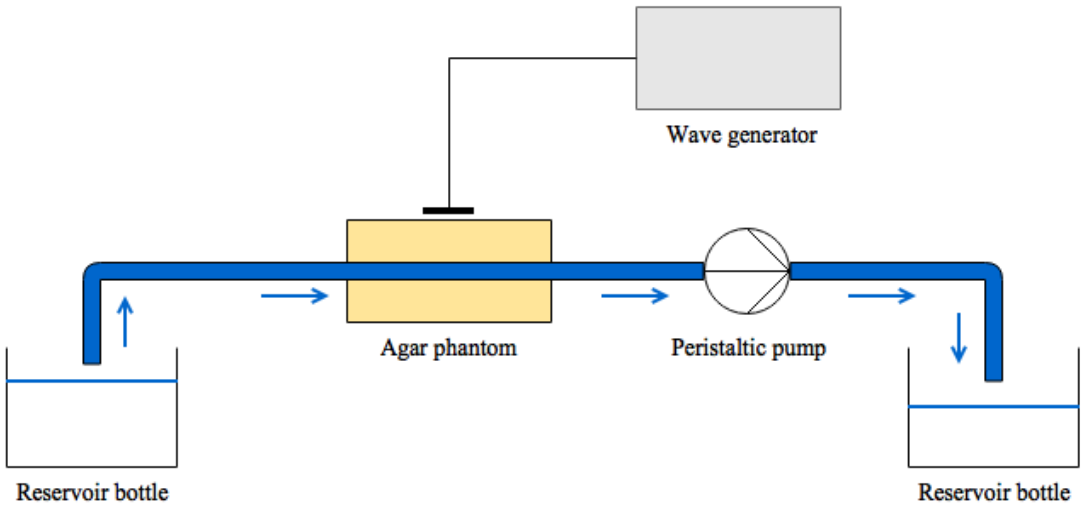

Figure 6: Scheme of the experimental setup.

2.2 Simplified numerical model

The simplified model used for evaluating the measurement outcome is an exact copy of the agar model created for the experiment. The numerical and agar models are identical in their dimensions and composition. Previously measured dielectric parameters of the different agar layers were also used as input in the numerical model in order to simulate the performed measurement as accurately as possible. The numerical model therefore consists of homogeneous muscle tissue of 10 cm height, a spherical tumour (d=2 cm) placed directly on a blood vessel (i.d. 2 mm) with its centre 2.7 cm under the surface, 8 mm layer of subcutaneous fat and 4.5 mm of skin. The base diameter of the cylindrical model is 20 cm and its thermophysical properties are presented in Table 1. Relative permittivity and electric conductivity of the agar mixtures used were measured and rest of the values were used from literature. The complete model can be seen on Fig. 7 and its individual parts are visualized in Fig. 9.

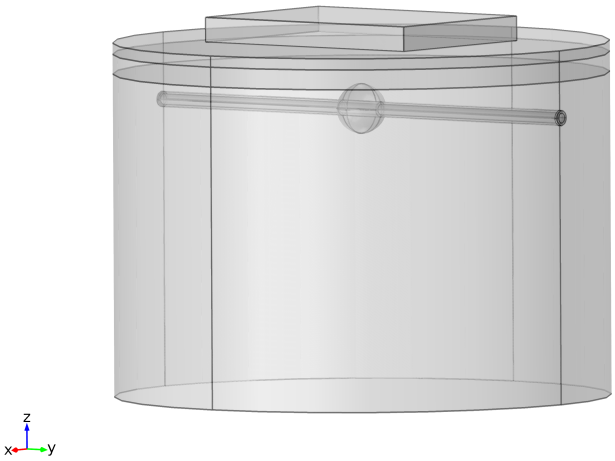

Figure 7: Cylindrical model with base diameter of 20 cm used for the simulations with 4.5 mm skin, 8 mm fat, and 10 cm muscle thicknesses. Vessel inner diameter is 2 mm with 1 mm wall thickness. Waveguide aperture dimensions are 10×7.5×3 cm.

The electrical field, blood flow velocity and temperature distribution were computed using Multiphysics (COMSOL AB, Stockholm, Sweden) – a finite element software. Three different computational modules were used in order to solve the combined bioheat transfer – Electromagnetic Waves, Laminar Flow and Bioheat Transfer. As temperature dependence of tissue parameters was not included in the final simulations, individual study steps could be separated and computed successively.

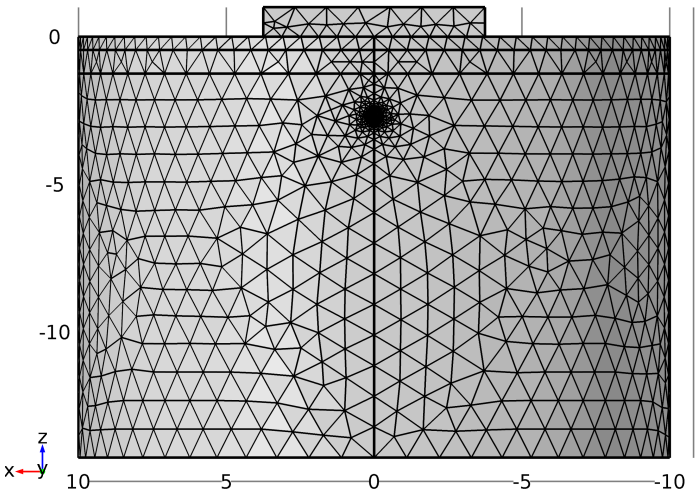

Figure 8: Resulting mesh of simplified computational model in x-z plane

Table 1: Thermal, biological and dielectric properties of phantom materials at 434 MHz and 23°C.

	$\sigma\ (\frac{\mathrm{S}}{\mathrm{m}})$	$\rho\ (\frac{\mathrm{kg}}{\mathrm{m}^3})$	$k\ (\frac{\mathrm{W}}{\mathrm{m\cdot K}})$	$\epsilon\ (-)$	$\omega_b\ (\frac{1}{\mathrm{s}})$	$C_p\ (\frac{\mathrm{J}}{\mathrm{kg\cdot K}})$
Muscle	0.72	1090 [18]	0.49 [18]	75.5	$6 \cdot 10^{-3}$ [5]	4200 [19]
Vessel Wall	10^{-15} [20]	940 [21]	0.33 [20]	2.3	$2.27 \cdot 10^{-4}$ [5]	1900 [20]
Blood	1.85	1000 [18]	0.61[22]	77.3	–	3617[18]
Fat	0.03	911 [18]	0.21 [18]	4.96	$5.98 \cdot 10^{-5}$ [5]	2348 [18]
Skin	0.75	1109 [18]	0.37 [18]	73.5	$1.6 \cdot 10^{-3}$ [5]	4200 [19]
Tumour	1.45	1040 [23]	0.64 [18]	59.5	$7.93 \cdot 10^{-4}$[5]	4200 [19]

Electromagnetic Waves and Laminar Flow were computed using a stationary study, whereas for Bioheat Transfer a Frequency-Transient study was used. The Frequency-Transient study duration was set to 2 minutes in order to match the experiment conditions. Power output of the wave generator was 100 W. The model was meshed with *Free tetrahedral* mesh set to *Finer* with minimal element size of 0.081 cm and maximal element size of 1.11 cm. Complete mesh consisted of 221069 elements. The resulting mesh can be seen in Fig. 8.

Temperature of all components of the numerical model was set to 23°C in order to match with the temperature during the experiment. Blood flow in the vessel was defined by inflow and outflow velocity – 1 cm/s.

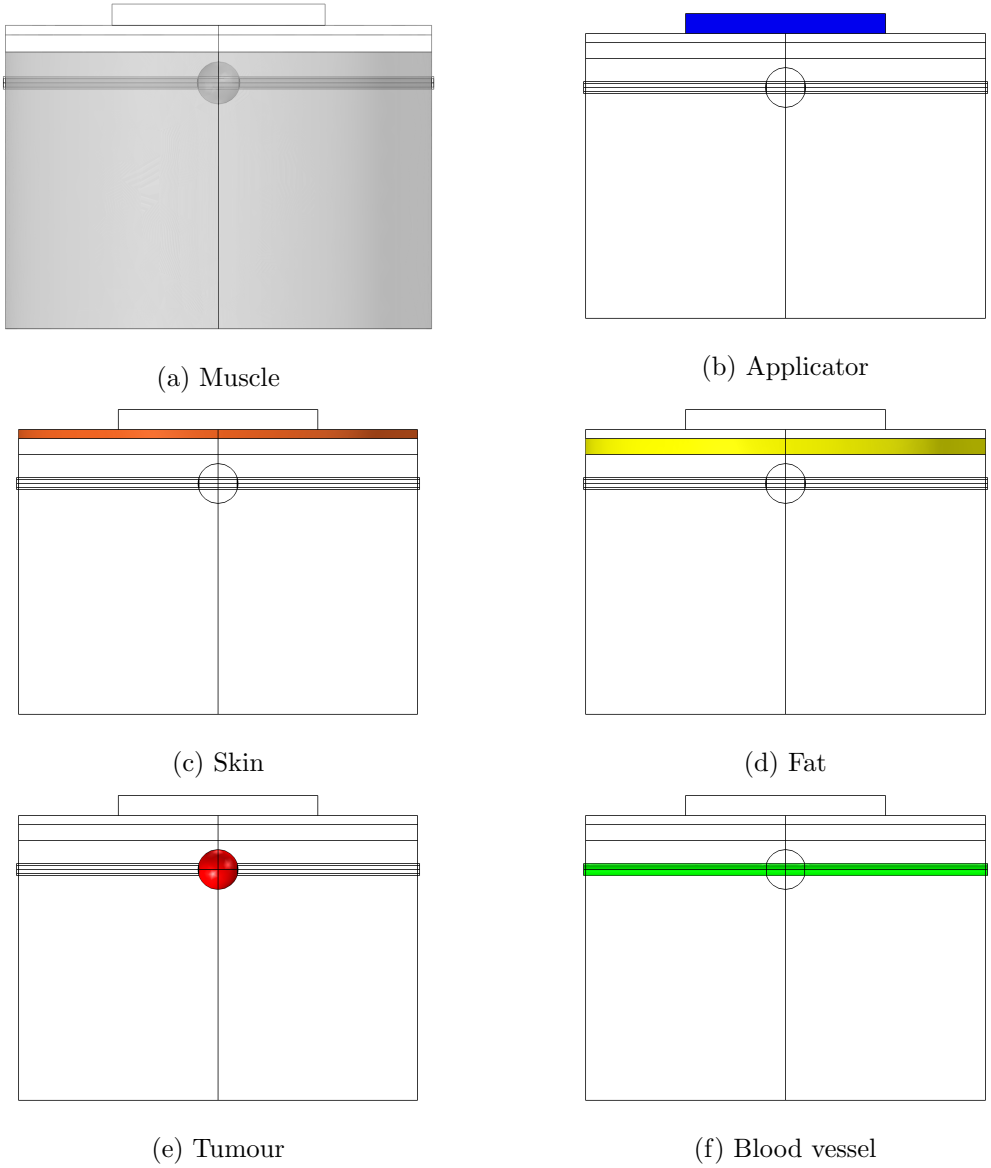

(a) Muscle

(b) Applicator

(c) Skin

(d) Fat

(e) Tumour

(f) Blood vessel

Figure 9: A visualisation of all components of the simplified numerical model.

2.3 Numerical model – tumour lying on a blood vessel

Multi-layer model representing tumour lying directly on a blood vessel consisted of 10 cm of muscle tissue, fat layer of 6 mm, 2 mm of skin, blood vessel with 5 mm i.d. and 1 mm wall thickness, tumour, microwave applicator and 1 cm of water bolus. Water bolus serves for cooling hotspots arising at the skin surface in contact with the microwave applicator. The resulting model can be seen in Fig. 10. Tumour size and its position under model surface varied; tumour diameters of 1 cm, 1.3 cm and 1.5 cm placed on a vessel in depths of 1.8 cm, 2 cm and 2.5 cm under the skin were used for the simulation. Depth of the tumour under the skin surface is always expressed for the centre of the tumour. Lateral dimensions of the model are 15×15 cm and waveguide aperture dimensions are 7.5×10×1 cm. All parts of the model are separately displayed in Fig. 12.

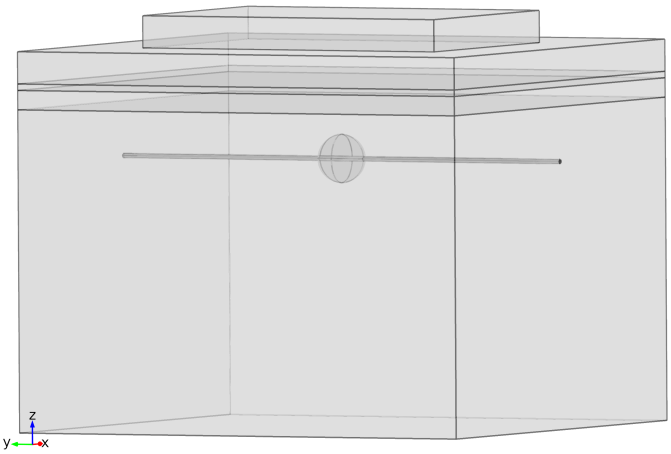

Figure 10: Model with blood vessel used for the simulations with 2 mm skin, 6 mm fat, 1 cm of water bolus and 10 cm muscle thickness. Lateral dimensions are 15×15 cm. Waveguide aperture dimensions are are 7.5×10×1 cm.

Temperature of all body tissues in the model was set to 37°C and the cooling bolus was embodied in a boundary condition with fixed $T_{bolus} = 18$°C. Blood flow velocity was set to 6 cm/s. All thermal and dielectric properties used in the simulation are displayed in Table 2.

Results were again obtained in COMSOL Multiphysics using successive simulations of Electromagnetic Waves, Laminar Flow and Bioheat Transfer. The model was meshed with *Free tetrahedral* mesh set to *Finer* with minimal element size of 0.06 cm and maximal element size of 0.83 cm. The resulting mesh can be seen in Fig. 11.

Table 2: Thermal, biological and dielectric properties of body tissues used in model at 434 MHz and 37°C.

	$\sigma\ (\frac{\mathrm{S}}{\mathrm{m}})$	$\rho\ (\frac{\mathrm{kg}}{\mathrm{m}^3})$	$k\ (\frac{\mathrm{W}}{\mathrm{m\cdot K}})$	$\epsilon\ (-)$	$\omega_b\ (\frac{1}{\mathrm{s}})$	$C_p\ (\frac{\mathrm{J}}{\mathrm{kg\cdot K}})$
Muscle	0.81 [18]	1090 [18]	0.49 [18]	56.9 [18]	$6 \cdot 10^{-3}$ [5]	3421 [18]
Vessel Wall	0.57 [18]	1102 [18]	0.46 [18]	46.7 [18]	$2.3 \cdot 10^{-4}$ [5]	3306 [18]
Blood	1.36 [18]	1050 [18]	0.52[18]	36.8 [18]	–	3617[18]
Fat	0.08 [18]	911 [18]	0.21 [18]	11.6 [18]	$6 \cdot 10^{-5}$ [5]	2348 [18]
Skin	0.70 [18]	1109 [18]	0.37 [18]	46.1 [18]	$1.6 \cdot 10^{-3}$ [5]	3391 [18]
Tumour	0.85 [23]	1040 [23]	0.51 [23]	57.9 [23]	$7.9 \cdot 10^{-4}$[5]	3950 [23]

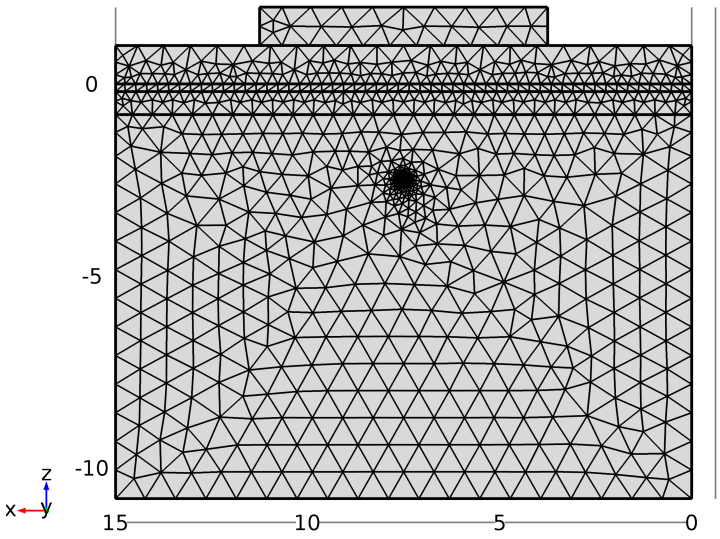

Figure 11: Resulting mesh of model of tumour lying directly on a blood vessel in x-z plane

All simulations were performed for an operating frequency of 434 MHz using stationary studies. Output power absorbed in the tissue together with temperature of water bolus were tuned aiming to ensure temperature distribution destroying the tumour tissue completely while causing the lowest possible damage to surrounding healthy tissue.

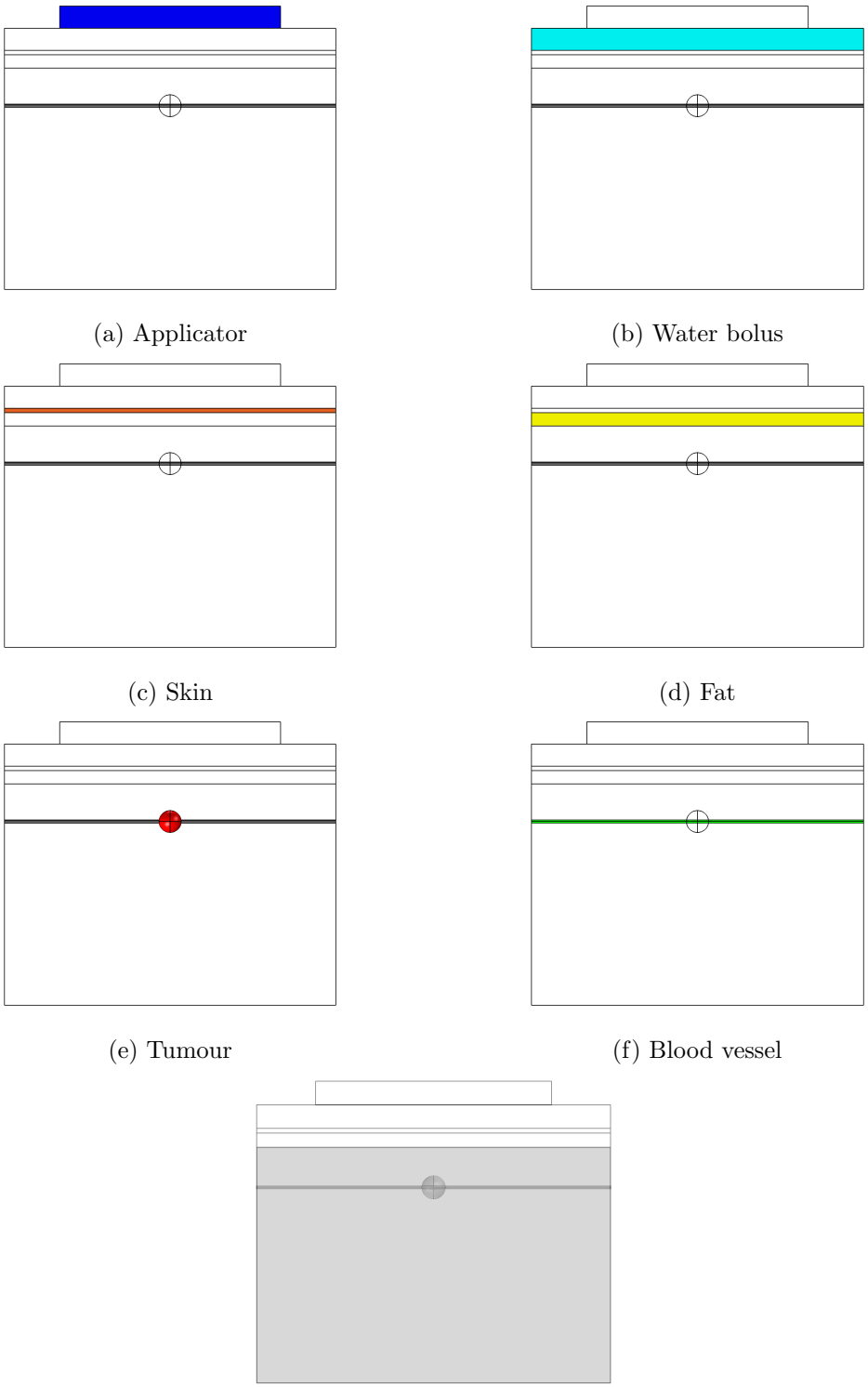

(a) Applicator

(b) Water bolus

(c) Skin

(d) Fat

(e) Tumour

(f) Blood vessel

(g) Muscle

Figure 12: A visualisation of all components of the numerical model of tumour being placed directly on a blood vessel.

2.4 Numerical model – tumour supplied from its surface

Numerical model of tumour being supplied by blood and other nutrients from its surface stands for a situation after vascular remodelling process causing local necrosis of the tissue inside the tumour. Model consists of 10 cm of muscle tissue, subcutaneous fat of 6 mm, 2 mm of skin, 1 cm of water bolus and tumour composed of two spheres. Outer sphere is well-perfused tumour tissue while inner sphere is necrotic with very low blood perfusion rate. Outer dimensions of this model as well as waveguide applicator size are the same as in the previous model. The entire model is displayed in Fig. 13 and its components are presented separately in Fig. 14. Tumour sizes and positions under the skin used in the simulations were the same as in model with tumour lying on a blood vessel. Therefore diameters of 1 cm, 1.3 cm and 1.5 cm with their centre placed in depths of 1.8 cm, 2 cm and 2.5 cm under the skin were studied in parametric simulations performed in COMSOL Multiphysics. As the tumour model consisted of two spheres, the core diameter was always adjusted according to the tumour diameter. Table 3 presents the core diameters matching to different tumour sizes used.

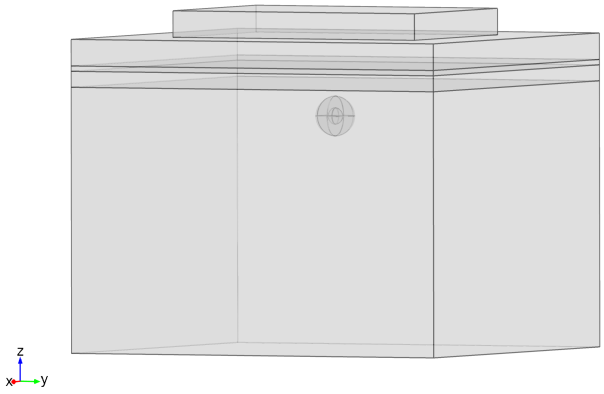

Figure 13: Model used for the simulations with 2 mm skin, 6 mm fat, 1 cm of water bolus and 10 cm muscle thickness. Lateral dimensions are 15×15 cm. Waveguide aperture dimensions are 7.5×10×1 cm.

Table 3: Diameters of tumour cores dependent on tumour diameters in the simulation.

Tumour diameter (mm)	**Core diameter (mm)**
10	4
13	5
15	6

Table 4: Thermal, biological and dielectric properties of body tissues used in model at 434 MHz and 37°C.

	$\sigma\,(\frac{\mathrm{S}}{\mathrm{m}})$	$\rho\,(\frac{\mathrm{kg}}{\mathrm{m}^3})$	$k\,(\frac{\mathrm{W}}{\mathrm{m\cdot K}})$	ϵ (–)	$\omega_b\,(\frac{1}{\mathrm{s}})$	$C_p\,(\frac{\mathrm{J}}{\mathrm{kg\cdot K}})$
Muscle	0.81 [18]	1090 [18]	0.49 [18]	56.9 [18]	$6 \cdot 10^{-3}$ [5]	3421 [18]
Fat	0.08 [18]	911 [18]	0.21 [18]	11.6 [18]	$6 \cdot 10^{-5}$ [5]	2348 [18]
Skin	0.70 [18]	1109 [18]	0.37 [18]	46.1 [18]	$1.6 \cdot 10^{-3}$ [5]	3391 [18]
Tumour perfused	0.85 [23]	1040 [23]	0.51 [23]	57.9 [23]	$7.9 \cdot 10^{-4}$[5]	3950 [23]
Tumour necrotic	0.89	1040 [23]	0.51 [23]	50	$7.9 \cdot 10^{-5}$	3950 [23]

The model was meshed with *Free tetrahedral* mesh set to *Finer* with minimal element size of 0.06 cm and maximal element size of 0.83 cm. The resulting mesh can be seen in Fig. 15. Stationary studies of Electromagnetic Waves and Bioheat Transfer for an operating frequency of 434 MHz were performed.

Boundary conditions and temperature settings were identical to the previous model and all thermal and dielectric properties of the simulated tissues are summarized in Table 4. Blood flow velocity through the blood vessel was 6 cm/s. Settings of water bolus temperature and output power absorbed in the tissue were manually tuned in order to obtain the desired temperature distribution. The aim of this setting was to maximize tumour volume heated to temperature above 41°C together with minimizing tissue volume heated to more than 45°C.

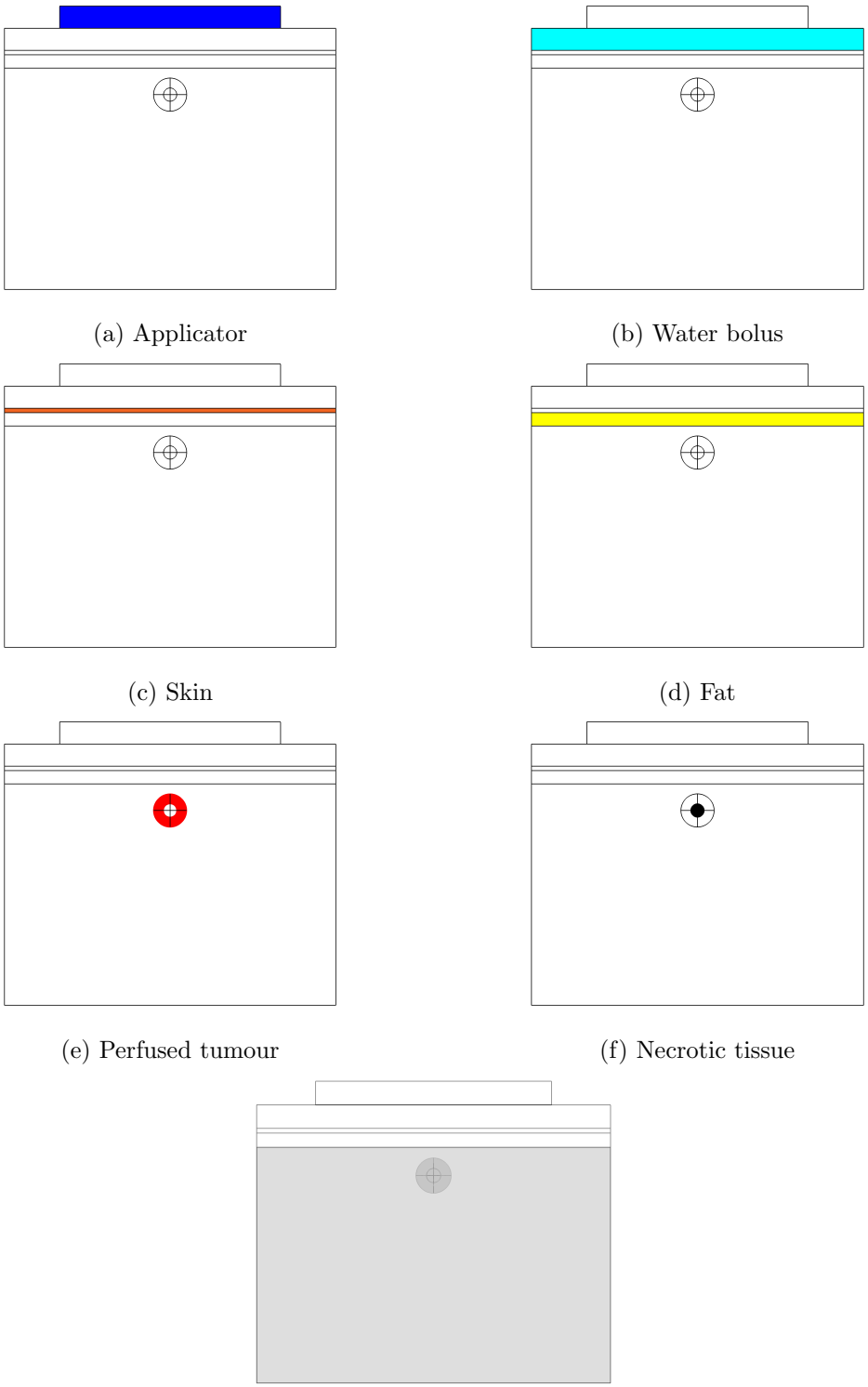

(a) Applicator

(b) Water bolus

(c) Skin

(d) Fat

(e) Perfused tumour

(f) Necrotic tissue

(g) Muscle

Figure 14: A visualisation of all components of the numerical model of tumour being supplied from its surface.

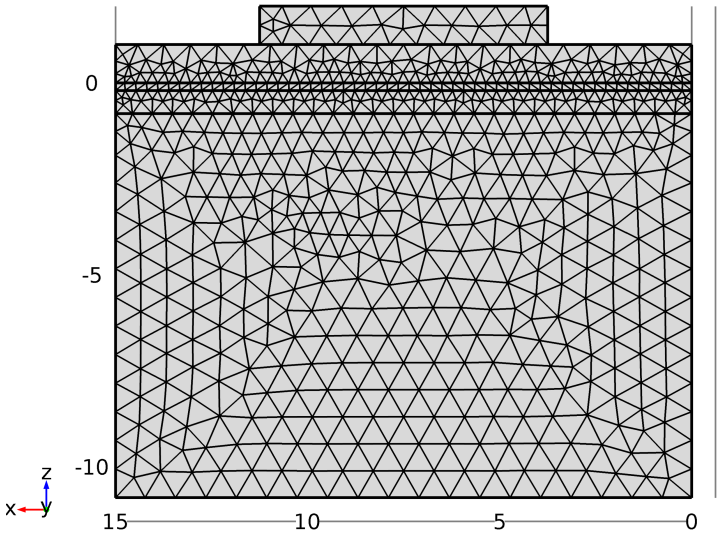

Figure 15: Resulting mesh of model of tumour being supplied from its surface in x-z plane.

3 Results

Experimental results as well as results of conducted numerical simulations are presented in this chapter. First, results from agar phantom experiment used for validating parameter settings in following simulations are presented and compared with results obtained from the matching simplified simulation. Further, results from simulations of both tumour types studied are introduced. For all simulations, graphical results of electromagnetic power loss density and temperature field distribution are displayed. Results are displayed in a vertical slice in the centre of the model. Colour range was manually unified in COMSOL Multiphysics, aiming the results to be mutually visually comparable. Result displaying blood flow in a vessel is presented only once (in Fig. 19) as the velocity profile was identical in all simulations. Tumour volume heated to temperature T>41°C, volume of surrounding tissue heated to more than 45°C as well as microwave generator power output and bolus temperature settings needed to achieve the presented temperature distribution are summarized in Tables 5 - 13.

3.1 Experimental validation of the numerical model

The temperature field distribution in the agar model cross section after application of microwaves over 2 minutes can be seen in Fig. 16. Tumour position was marked within the picture for better distinction.

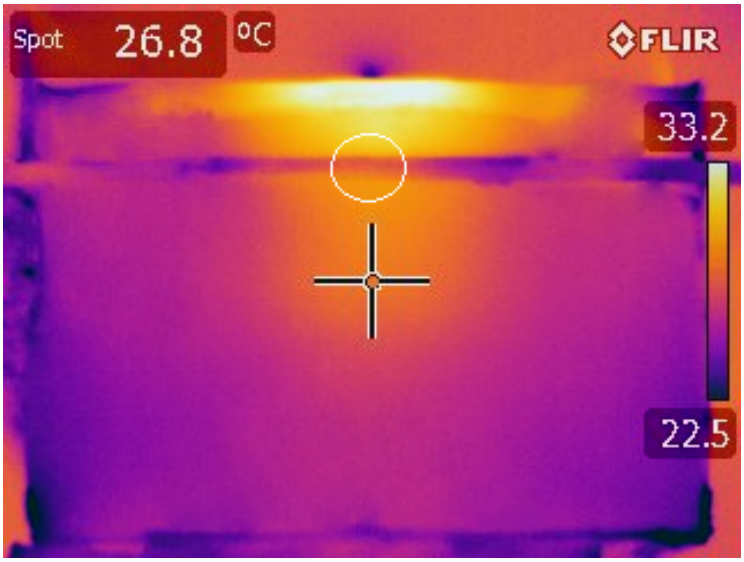

Figure 16: Thermographic image of agar phantom after microwave heating with marked tumour position, a cross section.

Outcome of the numerical simulation using parameters of the agar model is presented in Fig. 17. In Fig. 18, outcome of the numerical simulation with highlighted isothermal contours is displayed. Contours are figured in steps of 1°C. This figure serves for better comparison of the temperature field shapes in experiment and simulation.

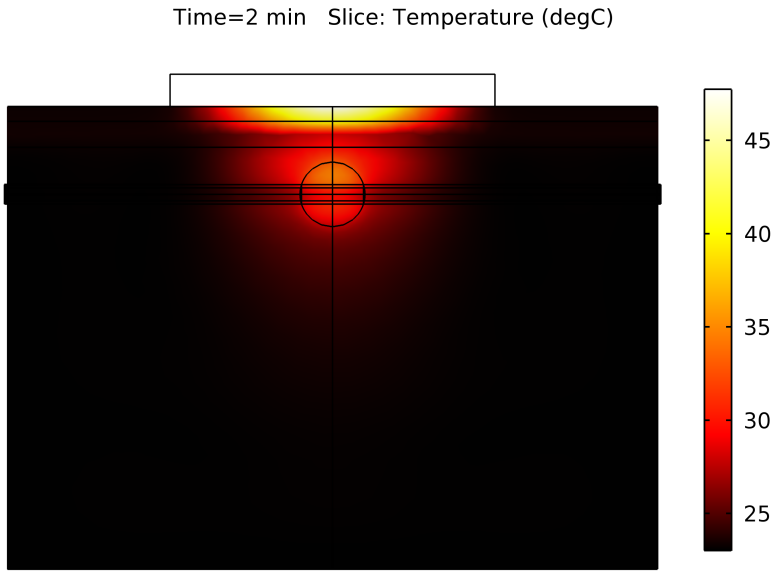

Figure 17: Simulated temperature distribution in model representing agar phantom, a cross sectional slice in y-z plane.

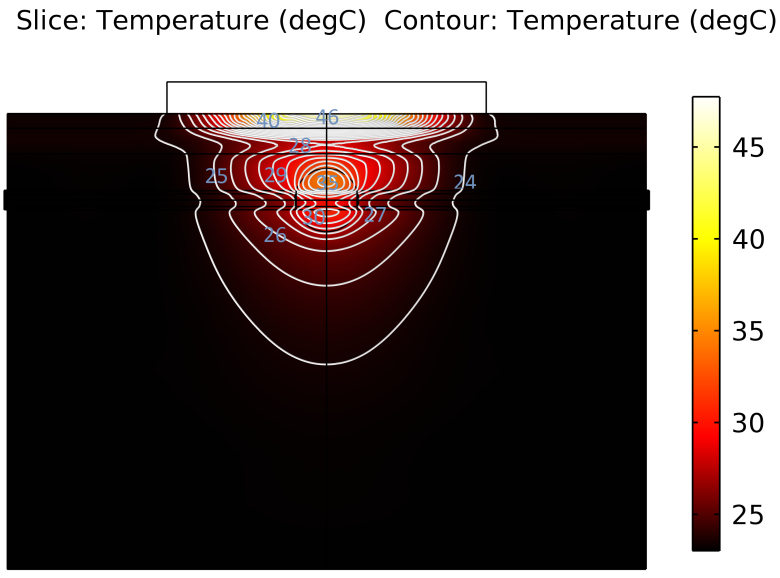

Figure 18: Simulated temperature distribution in model representing agar phantom with isothermal contours displayed, a cross sectional slice in y-z plane. Temperature of the contours is displayed in blue colour.

3.2 Tumour lying on a blood vessel

Results obtained from model of tumour lying on a blood vessel are presented in Tables 5 – 7 and Fig. 20 – 25. Each table contains results for one tumour depth (1.8, 2, or 2.5 cm) and all three tumour diameters (1, 1.3 and 1.5 cm). Volume of tumour heated to temperature higher than 41°C is displayed as well as volume of healthy tissue surrounding the tumour which might be damaged with temperature exceeding 45°C. Also output power and water bolus temperature settings are displayed in the tables. Colour range of temperature results was unified to $7 - 52$°C and range of electromagnetic power loss density to $0 - 9 \cdot 10^5$ W/m^3.

Result of blood flow distribution in a vessel is presented only once in Fig. 19, as the velocity profile was identical in all simulations including blood vessel.

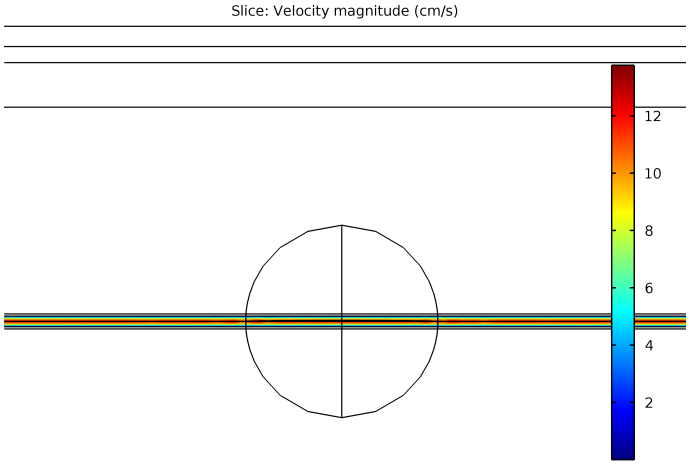

Figure 19: Velocity profile of blood stream through the model, close up of a cross sectional slice in y-z plane.

Table 5: Simulation results for tumour lying 1.8 cm under skin surface.

	Tumour volume (cm^3)	Tumour volume, T>41°C (cm^3)	Surrounding tissue, T>45°C (cm^3)	Output power (W)	Bolus temperature (°C)
d=1.0 cm	0.5	0.5	11.6	58	10
d=1.3 cm	1.2	1.2	10.2	57	10
d=1.5 cm	1.8	1.8	9.8	56	10

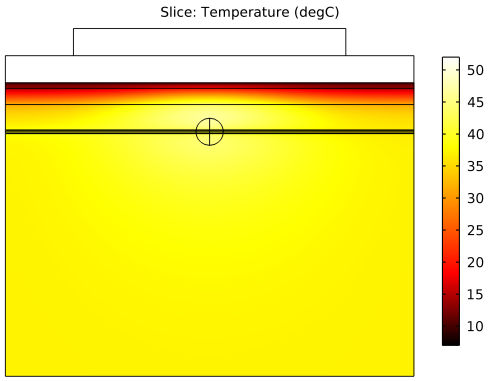

(a) d=1 cm

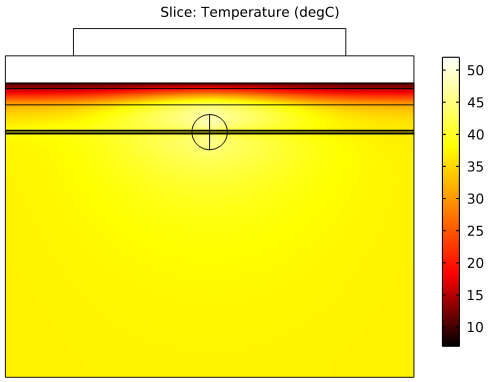

(b) d=1.3 cm

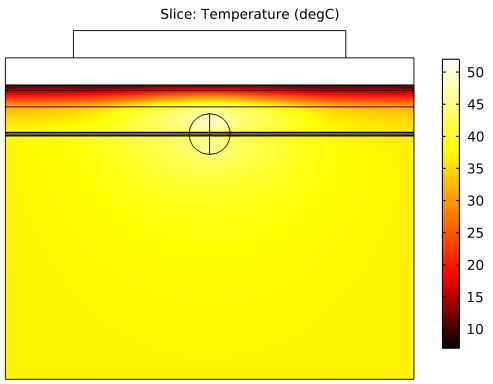

(c) d=1.5 cm

Figure 20: Temperature distribution in tumours lying on a blood vessel in depth of 1.8 cm, a cross sectional slice in y-z plane.

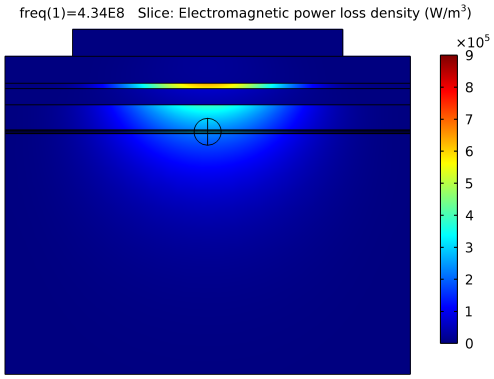

(a) d=1 cm

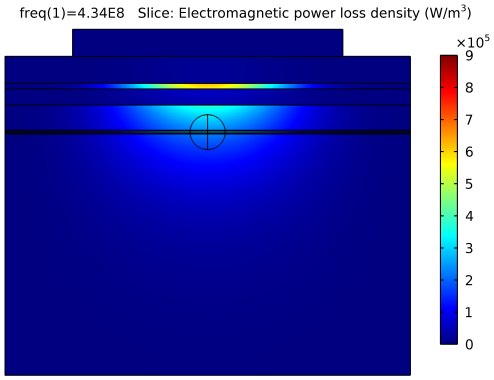

(b) d=1.3 cm

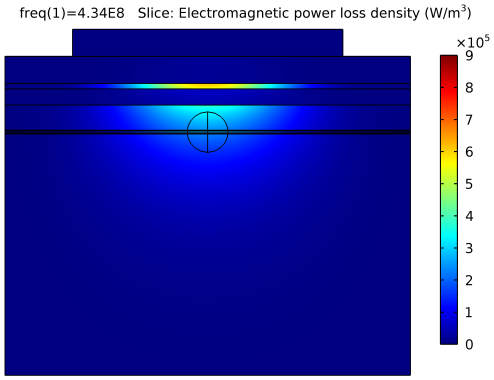

(c) d=1.5 cm

Figure 21: Electromagnetic power loss density in tumours lying on a blood vessel in depth of 1.8 cm, a cross sectional slice in y-z plane.

Table 6: Simulation results for tumour lying 2 cm under skin surface.

	Tumour volume (cm^3)	Tumour volume, T>41°C (cm^3)	Surrounding tissue, T>45°C (cm^3)	Output power (W)	Bolus temperature (°C)
d=1.0 cm	0.5	0.5	16.8	61	10
d=1.3 cm	1.2	1.2	15.8	59	12
d=1.5 cm	1.8	1.8	14.5	59	10

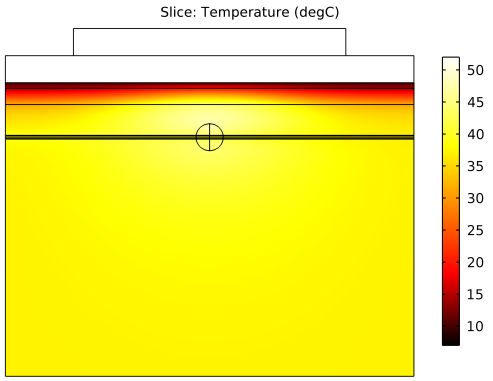

(a) d=1 cm

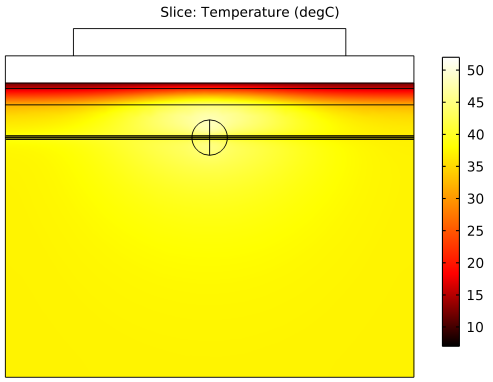

(b) d=1.3 cm

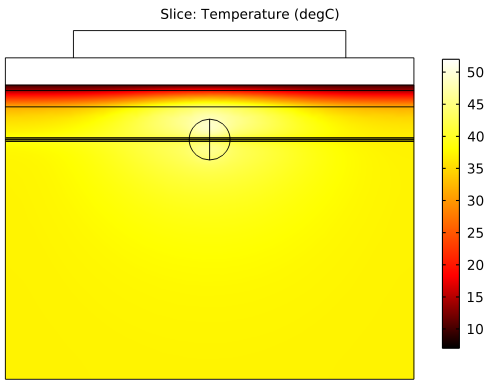

(c) d=1.5 cm

Figure 22: Temperature distribution in tumours lying on a blood vessel in depth of 2 cm, a cross sectional slice in y-z plane.

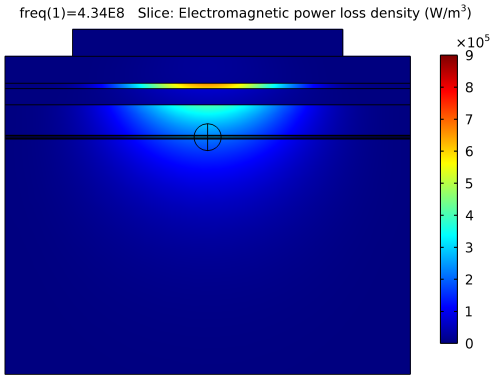

(a) d=1 cm

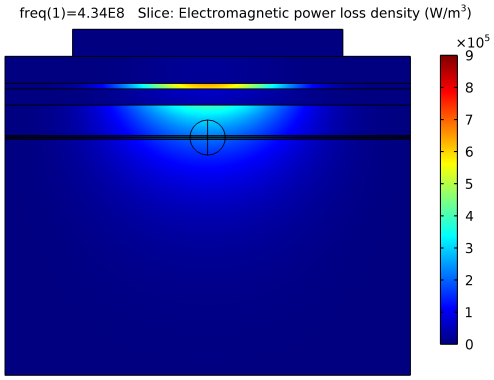

(b) d=1.3 cm

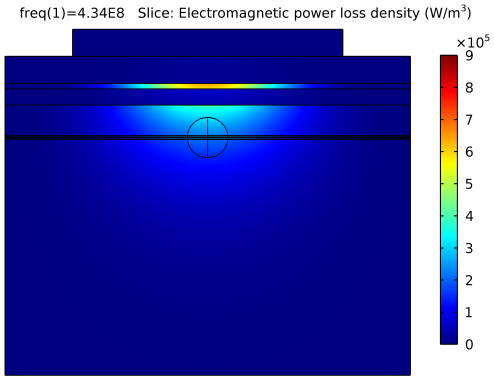

(c) d=1.5 cm

Figure 23: Electromagnetic power loss density in tumours lying on a blood vessel in depth of 2 cm, a cross sectional slice in y-z plane.

Table 7: Simulation results for tumour lying 2.5 cm under skin surface.

	Tumour volume (cm^3)	Tumour volume, T>41°C (cm^3)	Surrounding tissue, T>45°C (cm^3)	Output power (W)	Bolus temperature (°C)
d=1.0 cm	0.5	0.5	34.7	71	7
d=1.3 cm	1.2	1.2	34.5	70	10
d=1.5 cm	1.8	1.8	33.5	68	12

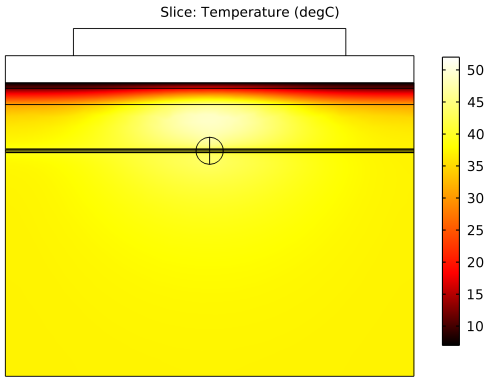

(a) d=1 cm

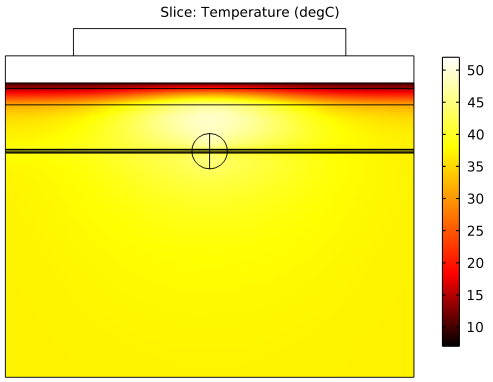

(b) d=1.3 cm

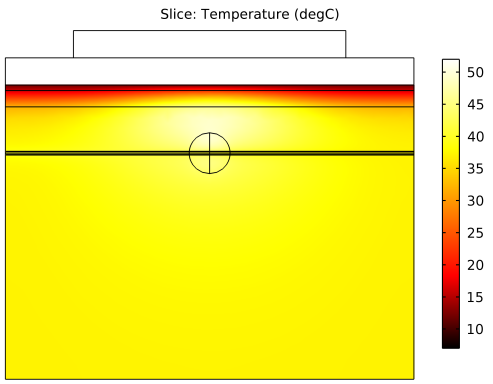

(c) d=1.5 cm

Figure 24: Temperature distribution in tumours lying on a blood vessel in depth of 2.5 cm, a cross sectional slice in y-z plane.

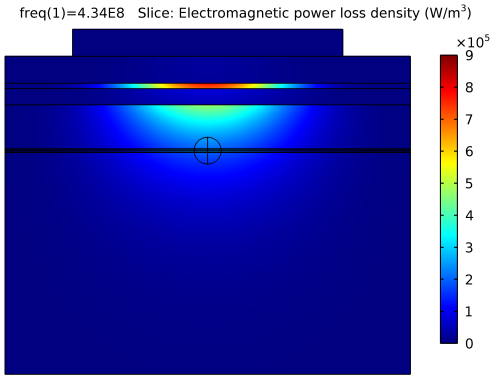

(a) d=1 cm

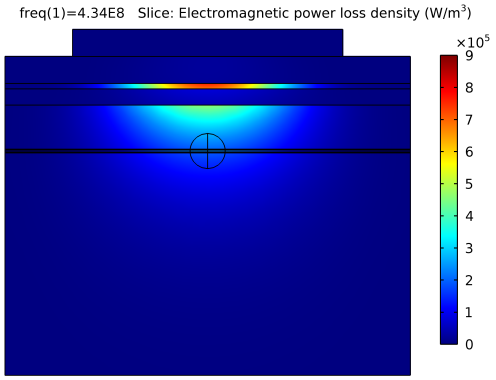

(b) d=1.3 cm

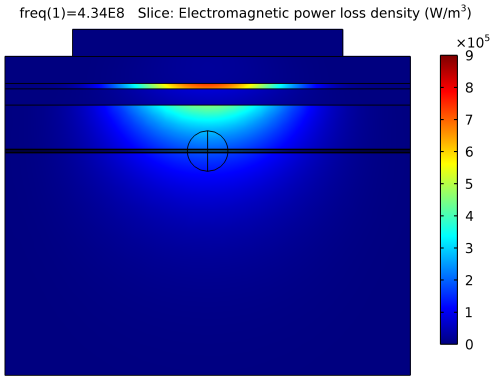

(c) d=1.5 cm

Figure 25: Electromagnetic power loss density in tumours lying on a blood vessel in depth of 2.5 cm, a cross sectional slice in y-z plane.

As it was not possible to heat the complete tumour volume to the desired temperature above 41°C without overheating some surrounding tissue, another set of results was created. Tables 8 – 10 present the percentage of tumour tissue, which could be heated to more than 41°C without damaging any surrounding tissue. Output power and water bolus temperature settings used to obtain these results are presented in the tables as well.

Table 8: Simulation results for tumour lying 1.8 cm under skin surface, without surrounding tissue damage.

	Tumour percentage, 41°C>T>45°C (%)	Output power (W)	Bolus temperature (°C)
d=1.0 cm	99.2	47	10
d=1.3 cm	99.6	45	10
d=1.5 cm	99.7	43	10

Table 9: Simulation results for tumour lying 2 cm under skin surface, without surrounding tissue damage.

	Tumour percentage, 41°C>T>45°C (%)	Output power (W)	Bolus temperature (°C)
d=1.0 cm	98.9	48	10
d=1.3 cm	99.2	45	12
d=1.5 cm	99.4	42	10

Table 10: Simulation results for tumour lying 2.5 cm under skin surface, without surrounding tissue damage.

	Tumour percentage, 41°C>T>45°C (%)	Output power (W)	Bolus temperature (°C)
d=1.0 cm	95.1	49	7
d=1.3 cm	97.2	46	10
d=1.5 cm	98.2	44	12

3.3 Tumour being supplied from its surface

In Fig. 26 – 31, temperature and electromagnetic power loss density distributions in tumour being supplied from its surface are presented. The value of depth under skin surface is always related to the centre of the tumour. Electromagnetic power loss density colour range was manually adjusted for all results to $0 - 5 \cdot 10^5$ W/m^3 and temperature range to $7 - 48$°C. These adjustments were made with the aim of easier visual comparison of the results. Output power needed for complete tumour destruction is mainly increasing with tumour diameter and depth under skin surface as displayed in Tables 11 – 13. It was possible to heat the complete tumour volume to the desired temperature above 41°C without overheating any surrounding tissue in all simulations of tumour being supplied from its surface.

Table 11: Simulation results for tumour lying 1.8 cm under skin surface.

	Tumour volume (cm^3)	Tumour volume, T>41°C (cm^3)	Surrounding tissue, T>45°C (cm^3)	Output power (W)	Bolus temperature (°C)
d=1.0 cm	0.5	0.5	0	27	13
d=1.3 cm	1.2	1.2	0	27	12
d=1.5 cm	1.8	1.8	0	27	12

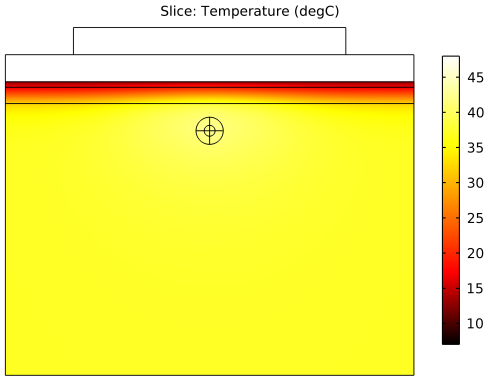

(a) d=1 cm

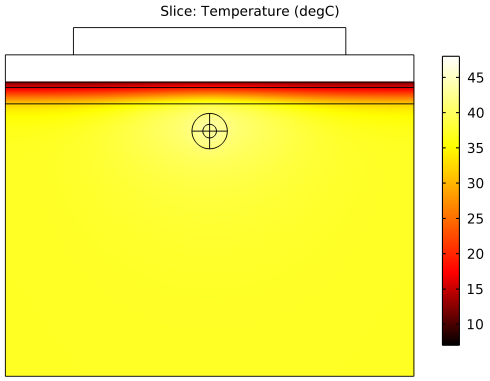

(b) d=1.3 cm

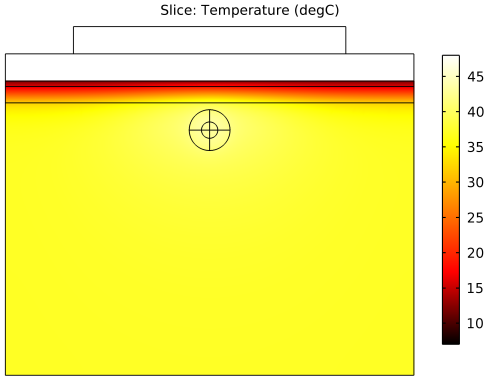

(c) d=1.5 cm

Figure 26: Temperature distribution in tumours being supplied from their surface in depth of 1.8 cm, a cross sectional slice in y-z plane.

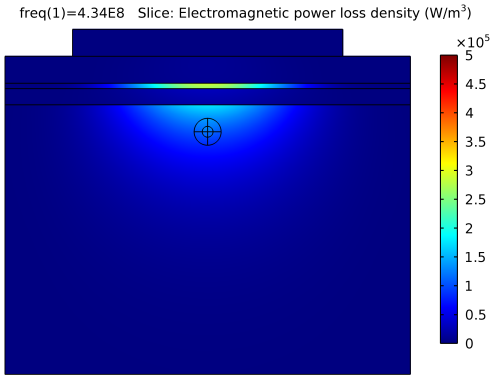

(a) d=1 cm

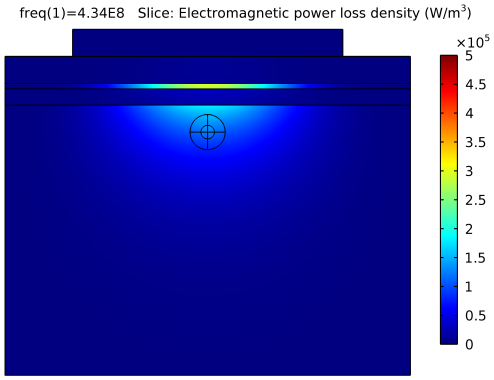

(b) d=1.3 cm

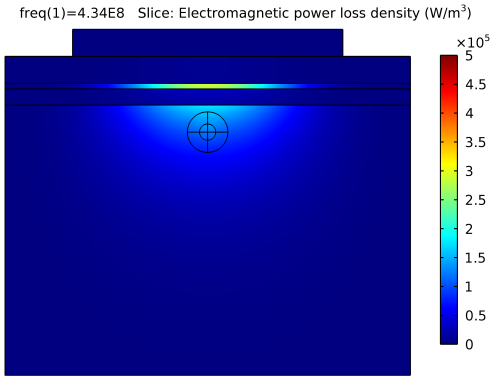

(c) d=1.5 cm

Figure 27: Electromagnetic power loss density in tumours being supplied from their surface in depth of 1.8 cm, a cross sectional slice in y-z plane.

Table 12: Simulation results for tumour lying 2 cm under skin surface.

	Tumour volume (cm^3)	Tumour volume, T>41°C (cm^3)	Surrounding tissue, T>45°C (cm^3)	Output power (W)	Bolus temperature (°C)
d=1.0 cm	0.5	0.5	0	28	13
d=1.3 cm	1.2	1.2	0	29	13
d=1.5 cm	1.8	1.8	0	30	12

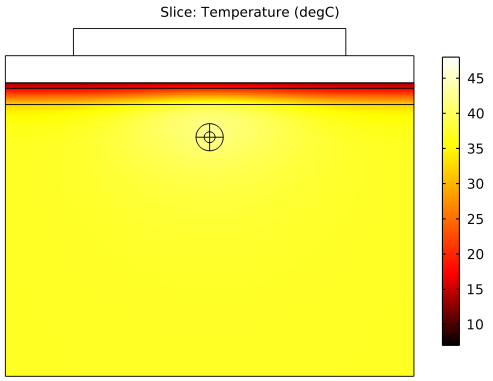

(a) d=1 cm

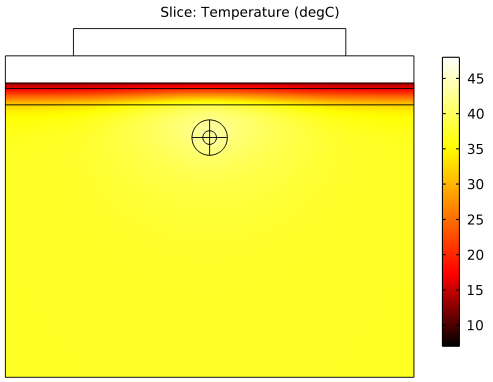

(b) d=1.3 cm

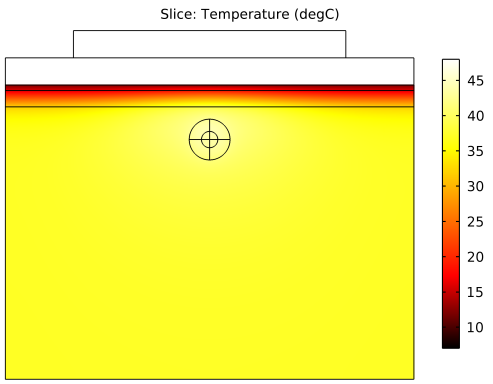

(c) d=1.5 cm

Figure 28: Temperature distribution in tumours being supplied from their surface in depth of 2 cm, a cross sectional slice in y-z plane.

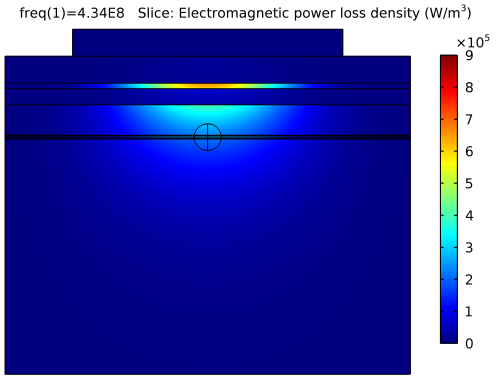

(a) d=1 cm

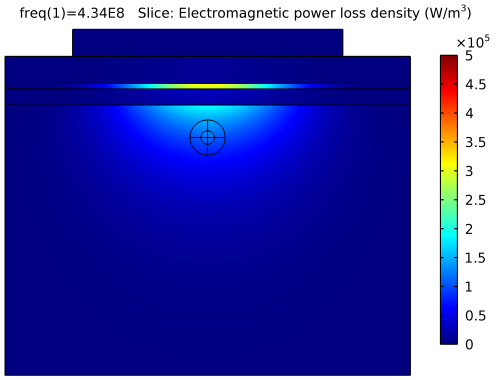

(b) d=1.3 cm

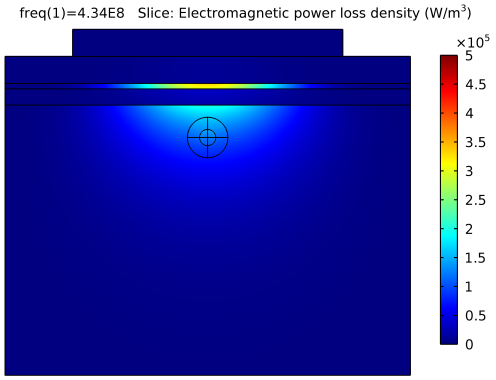

(c) d=1.5 cm

Figure 29: Electromagnetic power loss density in tumours lying being supplied from their surface in depth of 2 cm, a cross sectional slice in y-z plane.

Table 13: Simulation results for tumour lying 2.5 cm under skin surface.

	Tumour volume (cm^3)	Tumour volume, T>41°C (cm^3)	Surrounding tissue, T>45°C (cm^3)	Output power (W)	Bolus temperature (°C)
d=1.0 cm	0.5	0.5	0	28	13
d=1.3 cm	1.2	1.2	0	35	11
d=1.5 cm	1.8	1.8	0	36	10

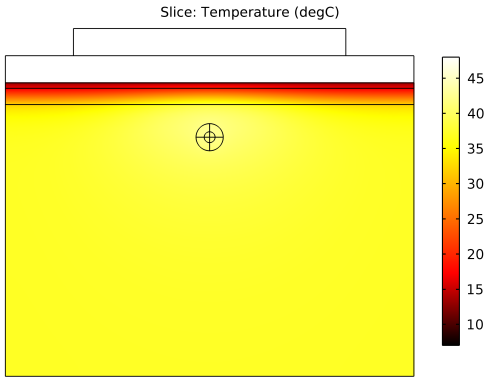

(a) d=1 cm

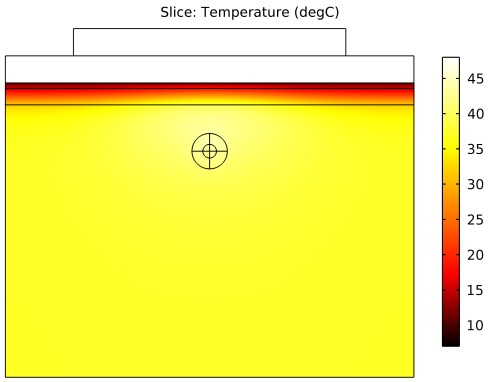

(b) d=1.3 cm

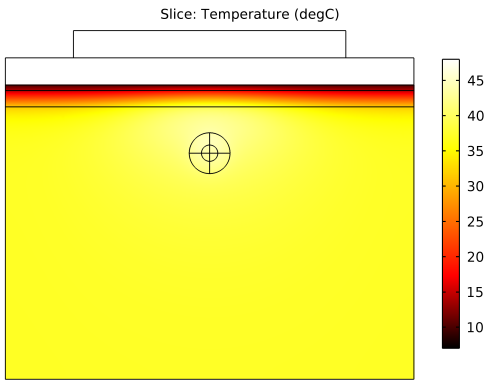

(c) d=1.5 cm

Figure 30: Temperature distribution in tumours being supplied from their surface in depth of 2.5 cm, a cross sectional slice in y-z plane.

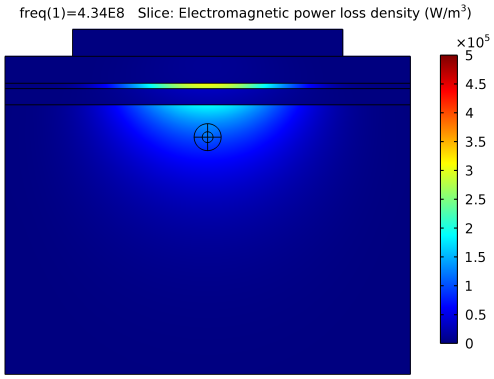

(a) d=1 cm

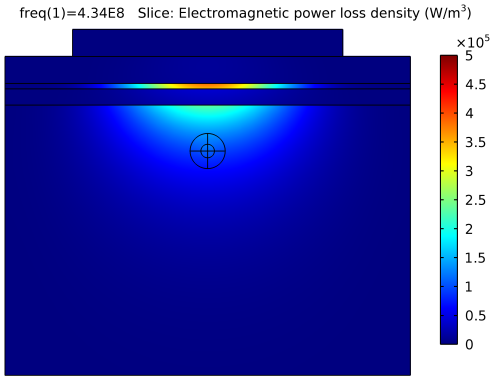

(b) d=1.3 cm

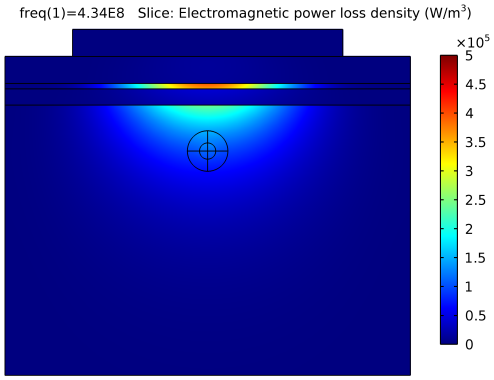

(c) d=1.5 cm

Figure 31: Electromagnetic power loss density in tumours being supplied from their surface in depth of 2.5 cm, a cross sectional slice in y-z plane.

4 Discussion

Major finding of this master's thesis is that there is a difference in temperature distribution after microwave heating of tumours with various blood supply. Results presented in the previous chapter illustrate the cooling effect of a blood vessel passing through a tumour. When compared with tumour supplied from its surface, it is also visible how the presence of blood vessel makes the therapy more demanding in terms of output power needed to destroy the tumour completely.

In order to be able to evaluate the simulated heating of tumour surrounded by healthy tissue it was necessary to use a heterogeneous model consisting of different layers representing various human body tissues. As the experimental validation of the simulations would not be possible using only a homogeneous model, a heterogeneous agar phantom was created.

When designing the agar model, it was crucial to find a suitable composition of all components in the model to imitate dielectric properties of real human body tissues. Some recipes found in literature turned out not to be suitable and had to be modified. Agar portion in the mixture representing tumour tissue was considerably increased in order to improve its consistency for the purpose of this experiment. After this adjustment, the final mixture was able to hold onto the PE tube, keep its round shape and was not being dissolved by the following agar mixture being poured over it. It was also found that there was no difference between dielectric parameters of mixtures created using distilled water and tap water. As all of the agar model components were drying out quickly, it was necessary to create the model on the instant to minimize the water loss. Model was covered with an impermeable cling film during time needed for each layer to solidify and also during transportation to the place of measurement. However, the measurement needed to be performed within a few hours after the model formation was complete. Model dimensions were designed large enough to let the microwaves be attenuated completely within the agar mass. This prevented reflections at boundaries and possible interference of reflected waves in the model.

Result of the experiment is presented in Fig. 16. As it was not possible to perform the experiment at body temperature (37°C), it was performed at room temperature (23°C) and initial conditions in the matching simulation were then adjusted accordingly. After application of microwaves on the agar model, it was necessary to take a thermographic

picture of a cross section. The model was therefore cut in half with a knife and a picture with thermographic camera was taken. As this process took us nearly 90 seconds, some heat was lost during the process. This explains the temperature difference between experiment and simulation outcome. As the shape of the temperature distribution is for the purpose of simulation validation more relevant than the maximal temperature, the original simulation outcome (Fig. 17) was also displayed with highlighted isothermal contours (Fig. 18). The isothermal contours in the figure were used for purposes of comparison with the experimental outcome. Compared, temperature distribution in the simplified simulation is analogous to the temperature distribution of the simulation outcome. Based on this we can consider simulation settings validated.

Simulations results of tumour lying directly on a blood vessel show that it was not possible to heat the studied tumours completely without damaging any surrounding tissue. In order to heat the complete tumour volume to temperature above 41°C, it was inevitable to have also regions of healthy tissue being heated to more than 45°C. Such temperature could lead to tissue ablation. However, in real human tissue, the tissue overheating would be smaller due to temperature dependent tissue perfusion. The temperature dependent vasodilatation mechanism was not considered in numerical simulations performed.

From presented results can be seen that microwave generator output power needed for complete destruction of tumour lying on a blood vessel is increasing together with decreasing tumour diameter. Also volume of overheated surrounding tissue increases as tumour diameter decreases. This phenomenon can be explained by the fact, that blood vessel diameter was the same for all tumour diameters used. As images of temperature distribution visualize, the cooling effect of blood flowing through the tumour applies only to close proximity of the vessel, as the same vessel diameter was used for all simulated tumour sizes. This implies, that the smaller the tumour diameter compared to the blood vessel diameter is, the bigger volume of it is being cooled during the therapy. Therefore more output power needs to be generated in order to heat the complete tumour volume to temperature above 41°C. The increased power output then causes unwanted overheating of healthy tissue surrounding the tumour.

The coolest place in the heated tissue was in all simulations an area at the vessel entrance to the tumour. This area shows therefore a high risk of not being destroyed completely during microwave hyperthermia treatment and causing later a potential tumour re-growth. As already mentioned, microwave hyperthermia treatment is usually being

combined with radiotherapy. Therefore it is possible to target this cooler area with a higher radiation dose. This approach should ensure complete tumour destruction and decrease the risk of a potential tumour re-growth.

As already stated, the presence of blood vessel in the tumour caused that it was not possible to destroy the tumour completely without causing any damage to healthy tissue. Therefore another set of simulations was performed. Their aim was to determine how much of the tumour tissue can be heated to more than 41°C without damaging any healthy tissue. The results presented in Tables 8 – 10 show that also here it was more difficult to heat small tumours. Percentage of tumour volume heated to desired temperature was increasing along with tumour diameter. It was also shown that with increasing depth of the tumour centre under skin surface the percentage of tumour heated to more than 41°C without healthy tissue overheating was decreasing. Although none of the simulated tumours lying on a blood vessel was destroyed completely, tumours in depth of 1.8 cm were heated of more than 99 %.

Simulation results of tumour being supplied from its surface indicate that the deeper the tumour is seated, the more output power was needed to heat it to desired temperature. This corresponds with the fact that microwaves are attenuated in the tissue, therefore more output power is required to penetrate deeper under the surface. In all simulations without blood vessel it was possible to achieve complete tumour heating to temperatures above 41°C without causing any damage to surrounding tissue.

When comparing both tumour types, it is visible that blood vessel passing through a tumour causes local cooling and generally worsens the temperature distribution. It also causes incomplete tumour heating and could therefore lead to later tumour re-growth. Compared to that, necrotic core in tumour being supplied from its surface did not create hot spots or cause any inhomogeneity in the temperature distribution.

Both simulations could be improved in the future by adding temperature dependency of tissue perfusion to the numerical models. This would refine the results for clinical use in patient-tailored hyperthermia treatment plan with high probability of tumour destruction and low risk of healthy tissue damage.

5 Conclusions

Two numerical models examining local microwave heating of different tumour types based on their blood supply were developed. They were successfully verified using an assembled experiment with an agar phantom. Differences in temperature distribution in both simulations during microwave hyperthermia treatment were found. We can say that blood vessel passing through a tumour has a considerable cooling effect and changes the temperature distribution in the treated area. It was shown that the presence of blood vessel makes the therapy more demanding in terms of output power needed to destroy the tumour completely. It was also found that necrotic core of tumour being supplied from its surface does not create any hot spots during therapy.

References

[1] GAUTHERIE, Michel*Interstitial, endocavitary and perfusional hyperthermia: methods and clinical trials.* Springer Science & Business Media, 2012. ISBN 9783642746420.

[2] CREZEE, J., LAGENDIJK, J. J. W. Temperature uniformity during hyperthermia: the impact of large vessels. *Physics in medicine and biology*. 1992, vol. 37, iss. 6, s. 1321.

[3] VRBA, Jan. *Lékařské aplikace mikrovlnné techniky*. Praha: Vydavatelství ČVUT, 2003. ISBN 80-01-02705-8.

[4] JAIN, R.K. a K. WARD-HARTLEY. Tumor Blood Flow-Characterization, Modifications, and Role in Hyperthermia. *IEEE Transactions on Sonics and Ultrasonics* [online]. 1984, vol. 31, iss. 5, s. 504–525 [cit. 2016-05-08]. DOI: 10.1109/T-SU.1984.31536. ISSN 0018-9537. Available from: http://ieeexplore.ieee.org/lpdocs/epic03/wrapper.htm?arnumber=1539612

[5] ERDMANN, Bodo, LANG, Jens, SEEBASS, Martin. Optimization of Temperature Distributions for Regional Hyperthermia Based on a Nonlinear Heat Transfer Modela. *Annals of the New York Academy of Sciences*. 1998, vol. 858, iss. 1, s. 36–46.

[6] LAGENDIJK, J J W. Hyperthermia treatment planning. *Physics in Medicine and Biology* [online]. 2000, vol. 45, iss. 5, s. R61–R76 [cit. 2016-05-08]. DOI: 10.1088/0031-9155/45/5/201. ISSN 0031-9155. Available from: http://stacks.iop.org/0031-9155/45/i=5/a=201?key=crossref.65cf1214f8e8236f027aaf0a1c23b2d1

[7] KOK, H. Petra, Johanna GELLERMANN, Cornelis A.T. VAN DEN BERG, Paul R. STAUFFER, Jeffrey W. HAND a Johannes CREZEE. Thermal modelling using discrete vasculature for thermal therapy: A review. *International Journal of Hyperthermia* [online]. 2013, vol. 29, iss. 4, s. 336–345 [cit. 2016-05-08]. DOI: 10.3109/02656736.2013.801521. ISSN 0265-6736. Available from: http://www.tandfonline.com/doi/full/10.3109/02656736.2013.801521

[8] STROHBEHN, John W. a Robert B. ROEMER. A Survey of Computer Simulations of Hyperthermia Treatments. *IEEE Transactions on Biomedical Engineering* [online]. 1984, vol. BME-31, iss.1, s. 136–149 [cit. 2016-05-08]. DOI: 10.1109/TBME.1984.325380. ISSN 0018-9294. Available from: http://ieeexplore.ieee.org/lpdocs/epic03/wrapper.htm?arnumber=4121724

[9] KOK, HP, P. WUST, PR STAUFFER, F BARDATI, GC VAN RHOON a J. CREZEE. Current state of the art of regional hyperthermia treatment planning: a review. *Radiation Oncology* [online]. 2015, vol. 10, iss. 1, - [cit. 2016-05-08]. DOI: 10.1186/s13014-015-0503-8. ISSN 1748-717x. Available from: http://www.ro-journal.com/content/10/1/196

[10] HOLASH, J. M. P. C., et al. Vessel cooption, regression, and growth in tumors mediated by angiopoietins and VEGF. *Science*. 1999, vol.284, iss. 5422, s. 1994–1998.

[11] RUOSLAHTI, Erkki. Specialization of tumour vasculature. *Nature Reviews Cancer*. 2002, vol. 2, iss. 2, s. 83–90.

[12] FOLKMAN, Judah. Tumor angiogenesis: therapeutic implications. *New england journal of medicine*. 1971, vol. 285, iss. 21, s. 1182–1186.

[13] TILKI, Derya, et al. Molecular imaging of tumor blood vessels in prostate cancer. *Anticancer research*. 2009, vol. 29, iss. 5, s. 1823–1829.

[14] VAUPEL, Peter. Tumor microenvironmental physiology and its implications for radiation oncology. *Seminars in Radiation Oncology* [online]. 2004, vol. 14, iss. 3, s. 198–206 [cit. 2016-05-08]. DOI: 10.1016/j.semradonc.2004.04.008. ISSN 10534296. Available from: http://linkinghub.elsevier.com/retrieve/pii/S1053429604000591

[15] HORSMAN, Michael R. Angiogenesis and vascular targeting: Relevance for hyperthermia. *nternational Journal of Hyperthermia* [online]. 2009, vol. 24, iss. 1, s. 57–65 [cit. 2016-05-08]. DOI: 10.1080/02656730701829710. ISSN 0265-6736. Available from: http://www.tandfonline.com/doi/full/10.1080/02656730701829710

[16] ORTEGA-PALACIOS, Rocío, et al. Measurement of breast-tumor phantom dielectric properties for microwave breast cancer treatment evaluation. In: *Electrical Engineering Computing Science and Automatic Control (CCE), 2010 7th International Conference on.* IEEE, 2010. s. 216–219.

[17] SPURNÝ, Pavel. *Návrh, výroba a testování fantomů pro mikrovlnné zobrazování.* Kladno, 2014. Bakalářská práce. České vysoké učení technické v Praze, Fakulta biomedicínského inženýrství.

[18] HASGALL P.A., Di GENNARO F., BAUMGARTNER C., NEUFELD E., GOSSELIN M.C., PAYNE D., KLINGEN A., KUSTER N. IT'IS Database for thermal and electromagnetic parameters of biological tissues. Version 3.0 [online].

September 01, 2015 [cit. 2016-05-08]. DOI: 10.13099/VIP21000-03-0. Available from: www.itis.ethz.ch/database

[19] YADAV, Satyendra. *Determination of thermal conductivity of tissue mimicking gel.* 2013. PhD Thesis. National Institute of Technology Rourkela.

[20] Professional Plastics. *Professionalplastics.com* [online]. 2016 [cit. 2016-03-24]. Available from: http://www.professionalplastics.com/PlasticMaterialsbyProperties

[21] All About Plastic Moulding. *Plasticmoulding.ca* [online].[cit. 2016-03-24]. Available from: http://www.plasticmoulding.ca/polymers/polyethylene.htm

[22] PITZER, Kenneth S., PEIPER, J. Christopher, BUSEY, R. H. Thermodynamic properties of aqueous sodium chloride solutions. *Journal of Physical and Chemical Reference Data.* 1984, vol. 13, iss. 1, s. 1–102.

[23] DRIZDAL, Tomas, Margarethus M. PAULIDES, Citlalli J. TRUJILO-ROMERO a Gerard C. VAN RHOON. Prediction of temperature distribution for superficial hyperthermia treatment: Accuracy of temperature dependent blood perfusion model. In: *2014 44th European Microwave Conference* [online]. IEEE, 2014, s. 782-785 [cit. 2016-05-08]. DOI: 10.1109/EuMC.2014.6986551. ISBN 978-2-8748-7035-4. Available from: http://ieeexplore.ieee.org/lpdocs/epic03/wrapper.htm?arnumber=6986551

[24] LIN, James C. *Advances in electromagnetic fields in living systems.* New York: Plenum Press, 1994.

[25] RODRIGUES, Dario B., et al. Optimization of chest wall hyperthermia treatment using a virtual human chest model. In: *Antennas and Propagation (EuCAP), 2015 9th European Conference on.* IEEE, 2015. s. 1-5.

[26] GUIDELINE, ICNIRP. Guidelines for limiting exposure to time-varying electric, magnetic, and electromagnetic fields (up to 300 GHz). *Health Phys.* 1998, vol. 74, iss. 4, s. 494–522.

[27] HÖCKEL, Michael, VAUPEL, Peter. Tumor hypoxia: definitions and current clinical, biologic, and molecular aspects. *NCI Journal of the National Cancer Institute* [online]. 2001, vol. 93, iss. 4, s. 266–276 [cit. 2016-05-08]. DOI: 10.1093/jnci/93.4.266. ISSN 0027-8874. Available from: http://jnci.oxfordjournals.org/cgi/doi/10.1093/jnci/93.4.266

[28] ZETTER, PHD, Bruce R. Angiogenesis and tumor metastasis. *Annual review of medicine* 1998, vol. 49, iss. 1, s. 407–424.

[29] CHAPLAIN, M. A. J. Avascular growth, angiogenesis and vascular growth in solid tumours: The mathematical modelling of the stages of tumour development. *Mathematical and computer modelling*. 1996, vol. 23, iss. 6, s. 47–87.

[30] SHIH, Tzu-Ching, Hao-Li LIU a Allen Tzyy-Leng HORNG. Cooling effect of thermally significant blood vessels in perfused tumor tissue during thermal therapy. *International Communications in Heat and Mass Transfer* [online]. 2006, vol. 33, iss. 2, s. 135–141 [cit. 2016-05-11]. DOI: 10.1016/j.icheatmasstransfer.2005.08.003. ISSN 07351933. Available from: http://linkinghub.elsevier.com/retrieve/pii/S0735193305001466

[31] BALANIS, Constantine A. Advanced Engineering Electromagnetics, ed. Solution Manual, Wiley, 1989. Chapter 2. ISBN 0471621943.

[32] GABRIEL, Sami, LAU, R. W., GABRIEL, Camelia. The dielectric properties of biological tissues: III. Parametric models for the dielectric spectrum of tissues. *Physics in medicine and biology*. 1996, vol. 41, iss. 11, s. 2271.

[33] KECHAGIOGLOU, Ioannis. Uncertainty and confidence in measurement. In: *Proceedings of the 18th Panhellenic Conference on Statistics*. 2005, s. 441–449.

Attachments

A CD content

- Master's thesis.pdf
- Diploma thesis assignment.pdf
- Zadání diplomové práce.pdf
- Title of thesis.pdf
- Abstract.pdf
- Abstrakt.pdf
- Keywords.pdf
- Klíčová slova.pdf
- Numerical simulations

B Attachments

- Attachment n. 1: Measured dielectric parameters of agar model

Attachment n. 1: Measured dielectric parameters of agar model

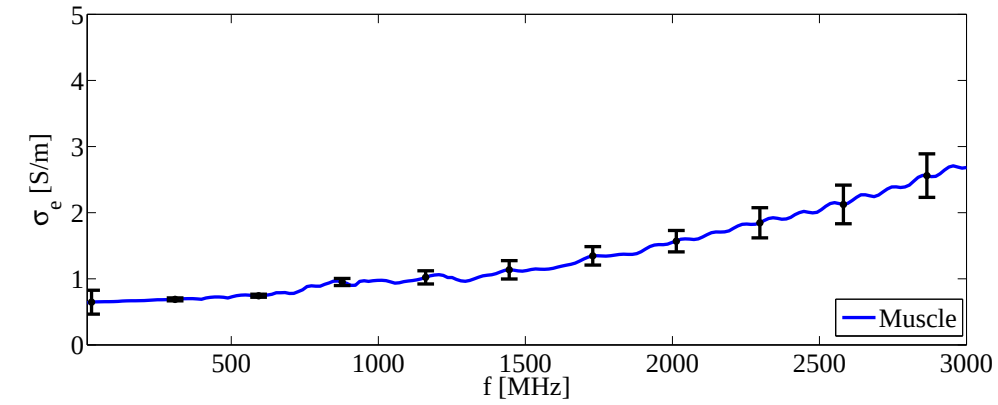

Figure A1: Measured conductivity of agar mixture representing muscle tissue with expanded measurement uncertainity (coverage factor k=2) figured.

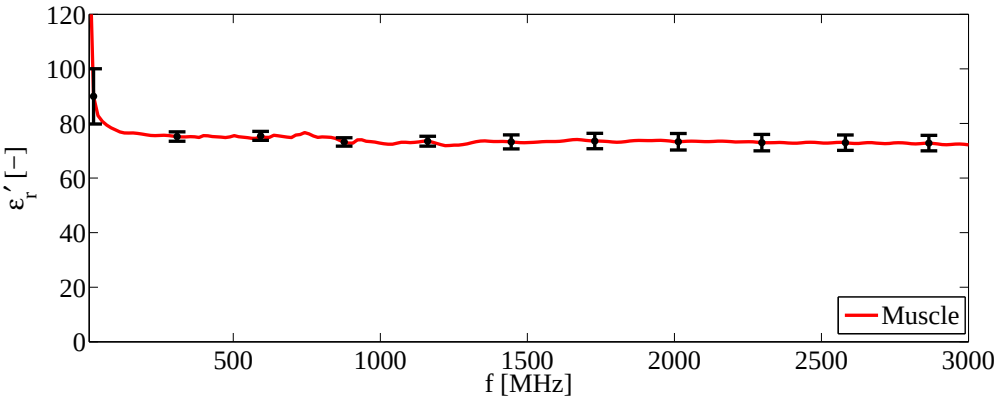

Figure A2: Measured permittivity of agar mixture representing muscle tissue with expanded measurement uncertainity (coverage factor k=2) figured.

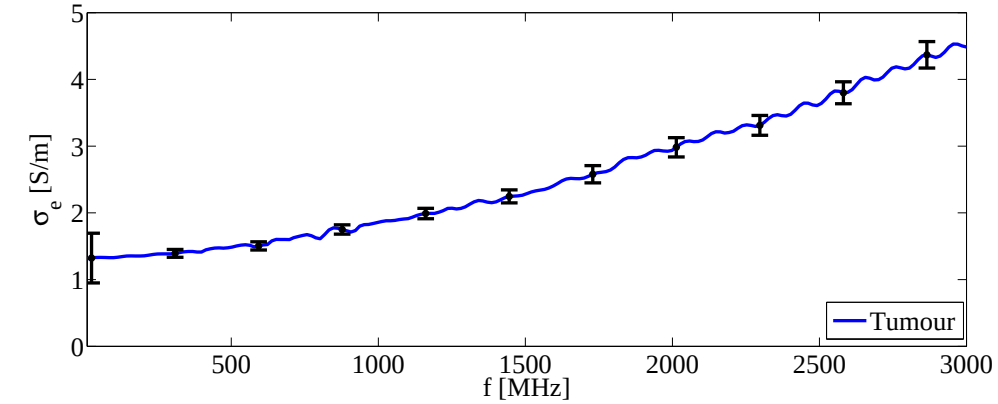

Figure A3: Measured conductivity of agar mixture representing tumour tissue with expanded measurement uncertainity (coverage factor k=2) figured.

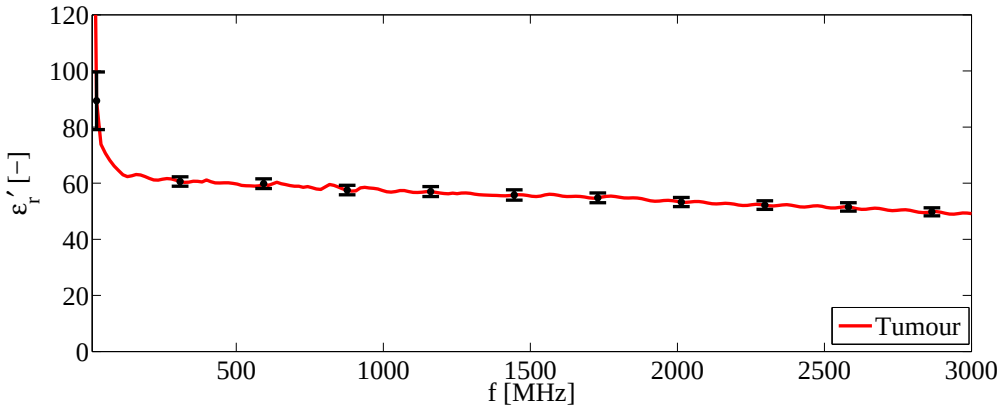

Figure A4: Measured permittivity of agar mixture representing tumour tissue with expanded measurement uncertainity (coverage factor k=2) figured.

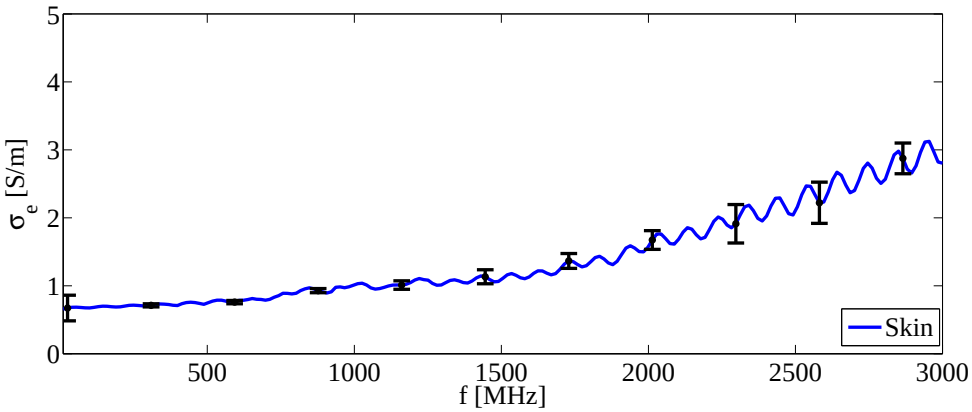

Figure A5: Measured conductivity of agar mixture representing skin with expanded measurement uncertainity (coverage factor k=2) figured.

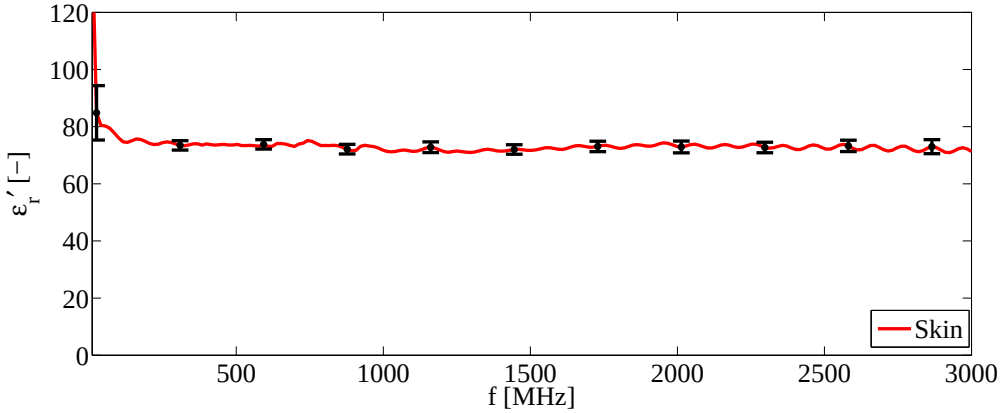

Figure A6: Measured permittivity of agar mixture representing skin with expanded measurement uncertainity (coverage factor k=2) figured.

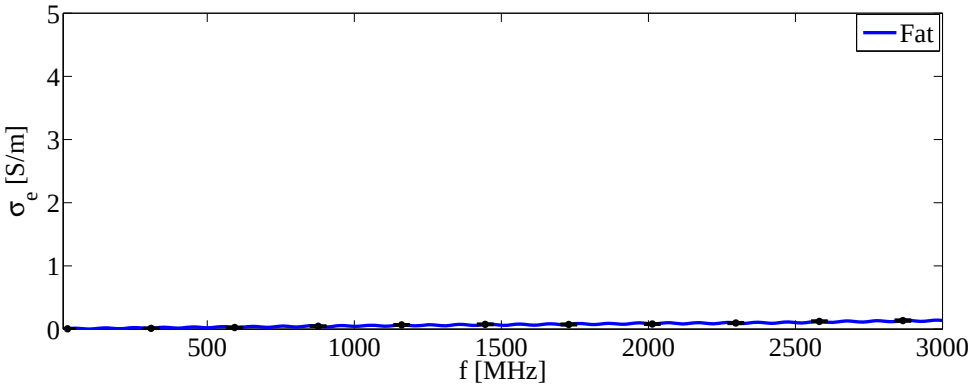

Figure A7: Measured conductivity of mixture representing subcutaneous fat with expanded measurement uncertainity (coverage factor k=2) figured.

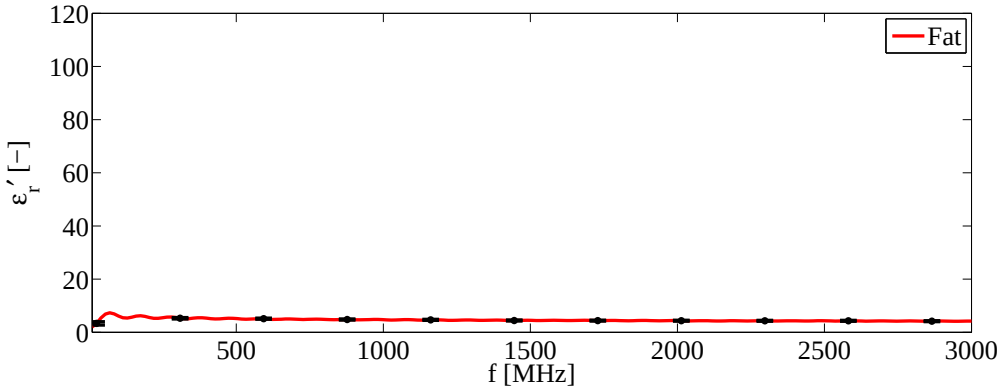

Figure A8: Measured permittivity of mixture representing subcutaneous fat with expanded measurement uncertainity (coverage factor k=2) figured.

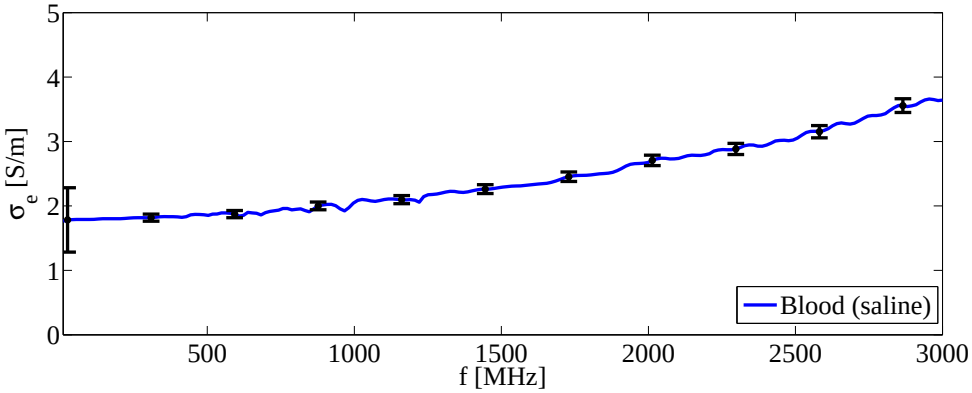

Figure A9: Measured conductivity of saline representing bloodwith expanded measurement uncertainity (coverage factor k=2) figured.

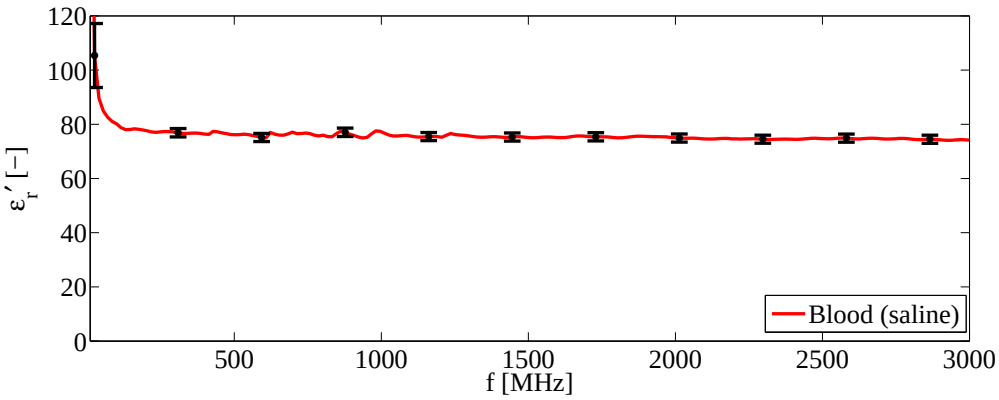

Figure A10: Measured permittivity of saline representing blood with expanded measurement uncertainity (coverage factor *k=2*) figured.